

# Comparison of dust optical depth from multi-sensor products and the MONARCH dust reanalysis over Northern Africa, the Middle East and Europe

Michail Mytilinaios<sup>1</sup>, Sara Basart<sup>2,3</sup>, Sergio Ciamprone<sup>1</sup>, Juan Cuesta<sup>4</sup>, Claudio Dema<sup>1</sup>, Enza Di Tomaso<sup>2</sup>, Paola Formenti<sup>5</sup>, Antonis Gkikas<sup>6,7</sup>, Oriol Jorba<sup>2</sup>, Ralph Kahn<sup>8</sup>, Carlos Pérez García-Pando<sup>2,9</sup>, Serena Trippetta<sup>1</sup>, and Lucia Mona<sup>1</sup>

<sup>1</sup>Consiglio Nazionale delle Ricerche-Istituto di Metodologie per l'Analisi Ambientale (CNR-IMAA), Tito Scalo, Italy

<sup>2</sup>Barcelona Supercomputing Center (BSC), Barcelona, Spain

<sup>3</sup>[World Meteorological Organisation \(WMO\), Science and Innovation Department, Geneva, Switzerland](#)

<sup>4</sup>Univ Paris Est Creteil and Université Paris Cité, CNRS, LISA, F-94010 Créteil, France

<sup>5</sup>Université Paris Cité and Univ Paris Est Creteil, CNRS, LISA, F-75013 Paris, France

<sup>6</sup>National Observatory of Athens-Institute for Astronomy, Astrophysics, Space Applications and Remote Sensing (NOA-IAASARS), Penteli, Greece

<sup>7</sup>[Research Centre for Atmospheric Physics and Climatology, Academy of Athens, Athens, Greece](#)

<sup>8</sup>Earth Sciences Division, NASA Goddard Space Flight Center, Greenbelt, Maryland, USA

<sup>9</sup>Catalan Institution for Research and Advanced Studies (ICREA), Barcelona, Spain

**Correspondence:** Michail Mytilinaios (michalis.mytilinaios@imaa.cnr.it)

**Abstract.** Aerosol reanalysis datasets are model-based observationally constrained continuous 3D aerosol fields with relatively high temporal frequency that can be used to assess aerosol variations and trends, climate effects and impacts upon socio-economic sectors, such as health. Here we compare and assess the recently published MONARCH high resolution regional desert dust reanalysis over Northern Africa, the Middle East and Europe (NAMEE) with a combination of ground-based observations and space-based dust retrievals and products. In particular, we compare the total and coarse dust optical depth (DOD) from the new reanalysis with DOD products derived from MODIS, MISR and IASI space-borne instruments. Despite the larger uncertainties, satellite-based datasets provide a better geographical coverage than ground-based observations, and the use of different retrievals and products allows for at least partially overcoming some single-product weaknesses in the comparison. Nevertheless, limitations and uncertainties due to the type of sensor, its operating principle, its sensitivity, its temporal and spatial resolution, and the methodology for retrieving or further deriving dust products, are factors that bias the reanalysis assessment. We, therefore, also ~~used~~use ground-based DOD observations provided by 238 stations of the AERONET network located within the NAMEE region as a reference evaluation dataset. In particular, prior to the reanalysis assessment, the satellite datasets were evaluated against AERONET, showing moderate underestimations in the vicinities of dust sources and downwind regions, whereas small or significant overestimations, depending on the dataset, can be found in the remote regions. Taking into consideration these results, the MONARCH reanalysis assessment ~~showed~~shows that total and coarse DOD simulations are consistent with satellite and ground-based data, capturing qualitatively the major dust sources in the area as well as the dust transport patterns. Moreover, the [MONARCH](#) reanalysis reproduces the seasonal dust cycle, identifying the

increased dust activity occurred in the NAMEE region during spring and summer. The quantitative comparison between the MONARCH reanalysis DOD and satellite multi-sensor products shows that the reanalysis tends to slightly overestimate the desert dust that is emitted from the source regions and underestimate the transported dust over the outflow regions, implying that the model removal of dust particles from the atmosphere, through deposition processes, is too effective. More specifically, small positive biases ~~were~~ are found over the Sahara Desert (0.04) and negative biases over the Atlantic Ocean and the Arabian Sea (−0.04), which constitute the main pathways of the long-range dust transport. Considering the DOD values recorded on average there, such discrepancies can be considered low as the low relative bias in the Sahara Desert ( $< 0.550\%$ ) and over the adjacent maritime regions ( $< +100\%$ ), certifies. Similarly, over areas with intense dust activity the linear correlation coefficient between the MONARCH reanalysis simulations and the ensemble of the satellite products is significantly high for both total and coarse DOD, reaching 0.8 over the Middle East, the Atlantic Ocean and the Arabian Sea, and exceeding it over the African continent. Moreover, the low relative biases and high correlations are associated with regions where large amounts of observations are available, allowing for robust ~~model~~ reanalysis assessment.

## 30 1 Introduction

Atmospheric desert dust is one of the major contributors to global aerosol loading and is the dominant component of atmospheric aerosols over large areas of Earth (Zender et al., 2004; Goudie and Middleton, 2006) with the Sahara Desert as the main contributor to the aerosol budget at global scale (Middleton and Goudie, 2001; Prospero et al., 2002; Ginoux et al., 2012a). Mineral dust particles, suspended in the atmosphere from arid and semi-arid regions, can remain aloft for periods ranging from several days to about a week, depending on their size (Prospero, 1999). Huge amounts of dust can be transported over great distances under favorable meteorological conditions, affecting regions hundreds to thousands of kilometers away (Mona et al., 2006; Papayannis et al., 2008, 2014; Flaounas et al., 2015; Gkikas et al., 2015; Ramaswamy et al., 2017; Yu et al., 2021).

The impact of atmospheric dust on the environment, health, and economies represents a major scientific and societal issue (UNCCD, 2022). Dust aerosols can interact with solar and thermal radiation and with clouds, affecting radiative forcing and precipitation formation and thus influencing Earth's weather and climate (Levin et al., 1996; Tegen et al., 1996; Myhre and Stordal, 2001; Slingo et al., 2006; Lambert et al., 2013; Myhre et al., 2013; Nabat et al., 2015; Karydis et al., 2017; Gkikas et al., 2018, 2019). Once the dust is deposited, by wet or dry deposition, it impacts both aquatic and terrestrial ecological systems through their biogeochemistry (~~Okin et al., 2004; Jickells et al., 2005; Painter et al., 2007; Lekunberri et al., 2010; Yu et al., 2015~~), e.g., dust contains micronutrients that can act as a fertilizer increasing primary productivity in the Amazon rain forest (~~Okin et al., 2004; Jickells et al., 2005; Painter et al., 2007; Bristow et al., 2010; Lekunberri et al., 2010; Yu et al., 2015~~). For countries in and downwind of arid regions, airborne sand and dust pose a significant threat to human and animal health (Gyan et al., 2005; Griffin, 2007; Kanatani et al., 2010; Mallone et al., 2011; Cadet et al., 2014; Pérez García-Pando et al., 2014; Querol et al., 2019; WHO, 2021) and to various socio-economic sectors, such as aviation, ground transportation, agriculture, infrastructure, solar energy and other industries (Goossens and Van Kerschaever, 1999; Sivakumar, 2005; Stefanski and Sivakumar, 2009; Mani and Pillai, 2010; Jiang et al., 2011; Weinzierl et al., 2012; Lekas et al., 2014; Costa et al., 2016; Al-Hemoud et al.,

2017; Middleton, 2017; Kosmopoulos et al., 2018; Miri and Middleton, 2022; Monteiro et al., 2022). It is therefore of great societal and scientific interest to better understand atmospheric dust processes, predict dust events and prevent or mitigate their unwanted impacts where possible.

A key parameter for tracking ~~the~~ airborne aerosols (including mineral dust) from satellite platforms and ground-based remote-sensing networks is aerosol optical depth (AOD). AOD is a quantitative measure of the attenuation of light as it is transmitted through the atmosphere, due to scattering and absorption by aerosols. As a result, AOD is proportional to the total amount of aerosol particles suspended in the atmosphere, providing important information about their concentration and variability; AOD spectral dependence is related to column-effective size distribution. Accordingly, coarse AOD is the fraction of the total AOD associated with coarse aerosol particles (~~i.e., approximate radius~~ larger than  $0.5 \mu\text{m}$  ~~in radius~~) in the atmosphere, and it is dominated by natural aerosols (~~i.e., sea salt and mineral dust; Carslaw et al., 2010~~) (e.g., sea salt and mineral dust; Carslaw et al., 2010). AOD wavelength-dependence is related to particle size, which has implications for climate, as direct radiative forcing induced by atmospheric aerosols depends strongly on particle size. Accordingly, studies suggest that fine dust generally produces cooling whereas coarse dust tends to produce warming (Tegen and Lacis, 1996; Miller et al., 2006; Mahowald et al., 2014; Kok et al., 2017), although there remains significant uncertainty in mineral dust properties and therefore their impact on climate projections (Myhre et al., 2013, see Fig. 8.17).

Over the last two decades, satellite and ground-based sensors have made systematic aerosol observations on a global scale, facilitating the integrated study of atmospheric aerosols and combining various measurement techniques and data analysis methods. Moreover, technological advancements nowadays allow for more detailed aerosol characterization, such as the estimation of mineral dust particle contributions to measured optical properties, providing an improved depiction of the atmospheric dust distribution globally (Kaufman et al., 2005; Liu et al., 2008, 2018; Giles et al., 2012; Peyridieu et al., 2013; Kahn and Gaitley, 2015; Gkikas et al., 2013, 2016; Marinou et al., 2017; Proestakis et al., 2018). Nevertheless, there are limitations regarding the spatiotemporal coverage of aerosol observations and aerosol typing. Ground-based measurements may provide high sampling frequency, e.g., one or more measurements per hour; however, they are limited to over-land surfaces and provide very limited spatial coverage. Further, the distribution of surface stations is not ideal in itself for studying the highly varying desert dust concentrations, and the regions most affected by sand and dust storms are generally not well supported by research infrastructures and networks (Benedetti et al., 2018). On the other hand, polar-orbiting satellite sampling capabilities above both land and sea are also limited, due to lower temporal resolution, as they obtain global coverage at best every 1 to 2 days (e.g., MODIS). For both surface and space-based aerosol remote sensing, ~~data availability measurement possibility~~ is affected by weather conditions (e.g., clouds and snow), and instruments that observe reflected or transmitted solar radiation (e.g., MODIS, MISR, AERONET sun-photometers) cannot obtain measurements during nighttime. Additionally, there is no single “best” aerosol satellite product globally, ~~e.g., and~~ some large differences are observed when comparing products from different sensors and algorithms (Sogacheva et al., 2020).

To fill these gaps, and overcome sparse coverage, low temporal resolution, and partial information provided by measurements, model simulations can be combined with observations within a data assimilation framework to estimate optimally the initial conditions for forecast models (analyses) and for the production of reanalysis datasets, i.e., complete and consistent

reconstructions of the atmosphere. Aerosol reanalysis datasets can accurately represent the spatial and temporal distribution of airborne dust over an extended period of time (Inness et al., 2013, 2019; Cuevas et al., 2015; Lynch et al., 2016; Gelaro et al., 2017; Yumimoto et al., 2017), reducing the estimated errors in numerical model simulations due to imperfect model dynamics as well as to uncertainties in the initial conditions and forcing fields, by means of assimilated observational constraint. A novel regional reanalysis of desert dust aerosol over the Northern Africa, the Middle East, and Europe (NAMEE) domain has been released recently by the Barcelona Supercomputing Center (Di Tomaso et al., 2021) for the period 2007–2016. The reanalysis was obtained using the MONARCH aerosol–chemical weather system and by assimilating a satellite AOD dataset that specifically constrains the dust component. The MONARCH dust reanalysis aims to provide reliable dust information at high temporal and spatial resolution, both near the surface and at upper levels. The reanalysis dataset consists of three-dimensional (3D) and two-dimensional (2D) variables covering a wide range of dust-related atmospheric parameters, including optical and microphysical dust properties along with dust deposition and solar radiation variables. Di Tomaso et al. (2022) describes the [MONARCH](#) reanalysis set-up as well as data assimilation diagnostics and provides a first basic evaluation of the reanalysis.

Here, we present a comprehensive assessment of the MONARCH reanalysis total and coarse mode dust optical depth (i.e., DOD and coarse DOD, respectively) at 550 nm against satellite-based mineral dust products retrieved or derived from different sensors (i.e., MODIS, MISR and IASI), along with ground-based AERONET AOD measurements. DOD is the model diagnostic variable directly constrained by observations through data assimilation and, therefore, is the primary focus of ~~our~~ [the MONARCH](#) reanalysis assessment. The validation of variables that are not directly constrained by observations such as the vertical extinction profile will be the subject of a companion study. Rather than use a single DOD reference dataset, we combine different DOD products that together provide better coverage of the ~~model~~[MONARCH](#)'s spatiotemporal domain. An additional advantage of using different observational reference datasets is the ability to perform cross-validation of ~~model~~[the MONARCH reanalysis](#) performance, based on the results obtained from each dataset. The total and coarse DOD products of the reference datasets were obtained following different retrieval techniques and assumptions; limitations of each dust characterization technique introduce uncertainties into the DOD retrievals. Nevertheless, by collating the comparison results obtained from different datasets, we can identify biases caused by retrieval uncertainties, and consider them in the final reanalysis assessment. To further investigate the reliability of the satellite-based DOD datasets, we also evaluated all products using an independent observational dataset (i.e., AERONET) as reference.

The following sections describe the assessment process and the results obtained. In Sect. 2 we present the main characteristics of the datasets used for the assessment of the MONARCH ~~DOD reanalysis~~[reanalysis DOD](#) along with a description of the applied methodology. In Sect. 3, validation of the satellite data using AERONET ground-based measurements is presented. Results from the MONARCH reanalysis assessment procedure are presented in Sect. 4, whereas in Sect. 5 the main findings and conclusions are summarized.

## 2 Datasets and methodology

The dust-related observational datasets selected for the MONARCH dust regional reanalysis assessment include remote-sensing products from ground-based networks (i.e., AERONET) and satellite sensors (i.e., MODIS, MIRS, and IASI). The selection of these remote-sensing-derived dust products considers the following requirements: i) the observational datasets should have sufficient temporal and geographical coverage over the [MONARCH](#) reanalysis dataset (i.e., NAMEE region and the period 2007–2016); ii) datasets must be consolidated in order to assure good quality data and to assess the associated errors; iii) ~~the data should be harmonized in terms of procedures and quality control within the specific dataset~~ [datasets must be homogeneous – i.e., no changes in the algorithm’s version or calibration of the instrument for the whole spatio-temporal domain – and harmonized – e.g., ground-based observations must be from international networks that implement a harmonized quality assurance and quality control procedure](#); lastly, iv) dust speciation is essential for the ~~dust-~~[MONARCH](#) reanalysis assessment. The latter means that the aerosol observational products should be related not to the total AOD, but specifically to its dust component, obtained through advanced products or through consolidated dust-filtering algorithms. Finally, in the assessment, it is important to consider that the observational and ~~modeling-reanalysis~~ datasets are usually available at different spatial and temporal resolutions, which implies that they must be collocated in terms of space and time before their comparison. Details about the dust AOD characterization and the spatiotemporal collocation methodology followed for every dataset are given in the next subsections.

### 2.1 MONARCH dust regional reanalysis

The MONARCH dust regional reanalysis represents the state of the art desert dust information over a domain covering the most prominent dust source areas in Northern Africa and the Middle East. This dataset has recently been released by the Barcelona Supercomputing Center (BSC) for a 10-year period, spanning from 2007 to 2016, over a spatial domain extending from 0° N to 70° N latitude and from ~~–30° E-W~~ to 70° E longitude. An extensive description of the [MONARCH](#) reanalysis set-up and dataset can be found in Di Tomaso et al. (2022). Here we summarize the main characteristics that are relevant for this study. The MONARCH reanalysis geographical domain includes some of the world’s main dust sources like the Sahara in Northern Africa, the Arabian Desert in the Middle East and the arid regions of Western Asia (Fig. 1), with the former emitting 50 % of total dust burden in the atmosphere (Ginoux et al., 2012b). It also includes maritime regions such as the Arabian Sea, the Mediterranean Sea and the northeastern Atlantic Ocean, over which long-range dust transport takes place frequently. A list of desert and arid regions, representing the major dust sources of the NAMEE region, is denoted by capital letters in Fig. 1. Figure 1 also shows the 10 sub-regions in which the MONARCH reanalysis domain is divided for evaluation purposes.

MONARCH reanalysis novelty includes its unprecedented spatial and temporal resolution, as well as the assimilation of an innovative DOD dataset covering all cloud-free and snow-free land surfaces, including areas particularly relevant for dust applications such as very bright reflective surfaces. Reanalysis fields are available at a 3-hourly time-step (starting every day at 03:00 UTC) and at a horizontal resolution of 0.1° latitude × 0.1° longitude in a rotated grid ( $\sim 10 \text{ km} \times 10 \text{ km}$  at the Equator). The reanalysis has been obtained using the Multiscale Online Non-hydrostatic Atmosphere Chemistry model (MONARCH;

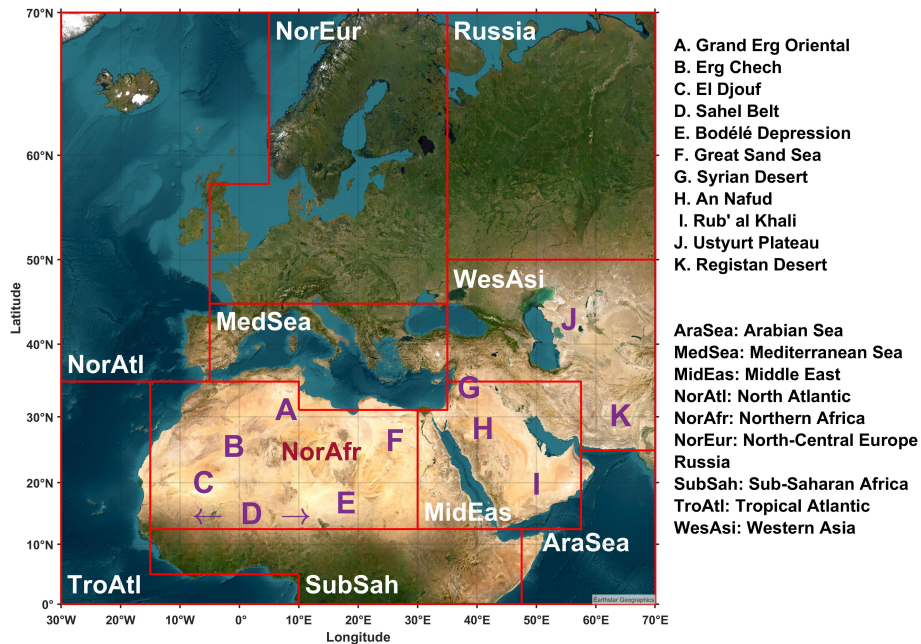


**Figure 1.** MONARCH reanalysis geographical domain (base map source: Esri, Earthstar Geographics, CNES/Airbus DS). The domain is divided into ten sub-regions; capital letters in purple mark the major deserts in Northern Africa, the Middle East and the Western Asia.

150 Pérez et al., 2011; Klose et al., 2021) and satellite coarse-mode DOD at 550 nm derived from the MODerate resolution Imaging Spectroradiometer (MODIS) instrument, operating aboard NASA's Aqua satellite. More specifically the dataset assimilated in the MONARCH reanalysis consists of gridded coarse DOD retrievals over land surfaces, including desert areas, derived from the MODIS Deep Blue aerosol products (Collection 6, Level 2; Hsu et al., 2004) according to the retrieval procedure described in Ginoux et al. (2010, 2012a) and Pu and Ginoux (2016). Data assimilation was performed by means of a local ensemble  
 155 transform Kalman filter data assimilation scheme with a four-dimensional extension (Hunt et al., 2007; Miyoshi and Yamane, 2007; Schutgens et al., 2010; Di Tomaso et al., 2017; Tsikerdekis et al., 2021; Escribano et al., 2022).

The [MONARCH](#) reanalysis dataset consists of upper-air [profile](#) variables such as dust mass concentration and extinction coefficient at 550 nm, surface fields such as accumulated dust dry and wet deposition and mass surface concentration, and total column fields like instantaneous total column dust load, DOD and coarse DOD at 550 nm. ~~Calculation of basic ensemble statistics was performed for each reanalysis variable~~ [The reanalysis has been produced by estimating model uncertainty from the realizations of the dust fields in a 12-member ensemble, where each ensemble member was generated using different meteorological initial and boundary conditions and dust emission schemes, along with additional perturbations in the model emission parameters. For each variable of the reanalysis a number of ensemble statistics is available](#), namely the ~~ensemble~~-arithmetic mean, standard deviation, median and maximum ~~;~~ ~~however, in this paper,~~ [of the ensemble members. In the present paper](#) we assess exclusively the reanalysis [ensemble](#) mean, as it is a more representative value than the median for describing the ensemble, as it considers all the members of the ensemble without excluding the outliers.

165



MONARCH follows a sectional approach for atmospheric dust, i.e., the size distribution is decomposed into eight size bins, corresponding to different dust particle ranges with particle radius ranging from 0.1  $\mu\text{m}$  (fine particles) to 10  $\mu\text{m}$  (coarse particles). The MONARCH reanalysis DOD is produced considering all eight model size bins, whereas the coarse mode DOD includes the five coarser size bins from 0.6 to 10  $\mu\text{m}$  in dust particle radius. For simplicity, hereafter, we refer to the MONARCH reanalysis [DOD](#) also as MONARCH [DOD](#).

## 2.2 MODIS-based dust product: MIDAS

The MODIS total and coarse DOD used in this study is based on the recently developed ModIs Dust AeroSol (MIDAS) dataset (Gkikas et al., 2020, 2021). MIDAS combines quality filtered AOD from MODIS [\(on-board-NASA's-Aqua-satellite\)-Dark-Target](#) [\(over-land-and-ocean\)-and-Deep-Blue-\(over-land\)](#) products [\(NASA's-Aqua-satellite, Collection 6.1, Level 2; Sayer et al., 2014\)](#) at swath level [\(Collection 6.1, Level 2\)](#), along with DOD-to-AOD ratios provided by the Modern-Era Retrospective analysis for Research and Applications version 2 (MERRA-2) reanalysis (Gelaro et al., 2017) to calculate the contribution of mineral dust particles to the overall AOD on the MODIS native grid. MIDAS coarse mode DOD is also derived using the MERRA-2 DOD fraction, and considers only particles with radius larger than 0.5  $\mu\text{m}$ . MIDAS provides columnar daily total and coarse DOD (at 550 nm) over all cloud-free and snow-free land and ocean surfaces, at fine spatial resolution ( $0.1^\circ \times 0.1^\circ$ ), and over a 15-year period (2003–2017).

The uncertainty of the MIDAS DOD dataset was estimated by taking into account the uncertainties of the MODIS AOD and MERRA-2 DOD-to-AOD ratio (Gkikas et al., 2021), which in turn were calculated by using AERONET AOD (Giles et al., 2019) and LIVAS (Amiridis et al., 2015; Marinou et al., 2017) dust fraction, respectively, as a reference. According to the uncertainty analysis performed, MIDAS uncertainties scale with DOD value (Gkikas et al., 2021, see Fig. 8); however, in terms of relative uncertainty the MIDAS DOD product is highly reliable over dust-rich regions [\( \$\sim 33\%\$  annual average in the regions with strongest DODs\)](#) and becomes more uncertain in areas where dust loading is infrequent. Although the MIDAS coarse DOD product is still under testing, it was used in this study after being evaluated against ground-based AERONET coarse DOD observations (Sect. 3).

Prior to the comparison, the MONARCH and MIDAS datasets were collocated in space and in time. First, MONARCH was re-gridded through bilinear interpolation, using the MIDAS grid as a reference. Regarding the temporal collocation, thanks to the wide MODIS swath ( $\sim 2330$  km), MIDAS provides near-global DOD retrievals every 1 to 2 days; consequently, MONARCH 3-hourly time-steps had to be averaged around Aqua's overpass time. Aqua follows a sun-synchronous, near-polar orbit, crossing the Equator once during daytime at  $\sim 13:30$  local time (LT). ~~As MONARCH outputs are given in UTC, it was necessary to convert 13:30 LT to UTC units, which depends on longitude. The MONARCH spatial domain contains eight time-zones (15 degrees of longitude constitute one time-zone) from  $-2$  hours to  $+5$  hours, implying that Aqua/MODIS takes measurements over the MONARCH domain between 08:30 UTC ( $70^\circ$  E) and 15:30 UTC ( $-30^\circ$  E). Hence, for a given longitude (assume  $43^\circ$  E) related to a certain time-zone (i.e.,  $+3$  hours), and hence the MONARCH DOD was temporally averaged around MODIS acquisition time (i.e., 10:30 UTC) that time using the two nearest MONARCH timeslots (i.e., 09:00 and 12:00 UTC).~~

### 2.3 MISR dust product

Multi-angle Imaging SpectroRadiometer (MISR) is an imaging instrument, which provides aerosol observations on a global scale since 2000 (Diner et al., 1998). The MISR instrument consists of nine cameras observing at nine different view angles (between  $-70.5^\circ$  and  $70.5^\circ$ ), and in four different wavelengths (446.4 nm, 557.5 nm, 671.7 nm and 866.4 nm). Apart from the AOD retrievals in the four spectral bands, the variations between the reflectance acquired from a very large range of scattering angles can provide information about aerosol microphysical properties such as particle size, shape, and single-scattering albedo by considering the appropriate particle optical models (Kahn et al., 1998, 2001; Kahn and Gaitley, 2015). In particular, MISR's sensitivity to the characteristics of the aerosol scattering phase function enables it to distinguish between the non-spherical and spherical particles, making it possible to separate mineral dust aerosols from other aerosol components (Kahn et al., 1997). Thus, the AOD fraction of the non-spherical particles, consisting of randomly oriented non-spherical grains or ellipsoids, can be considered equivalent to the DOD with relative certainty, especially over dark-water surfaces (Kalashnikova and Kahn, 2006). ~~Generally, Many studies show that MISR's sensitivity to DOD depends on the surface type and~~ like nearly all passive satellite aerosol remote-sensing, MISR ~~AOD~~ retrievals are less reliable over bright surfaces (Kahn et al., 2010). ~~Specifically, MISR over-land retrievals tend to underestimate DOD in dust-rich areas and have greater uncertainties compared to MISR over-water DOD~~; therefore, for the MONARCH DOD comparison we used exclusively dark-water retrievals, which are exceedingly sensitive to aerosol non-sphericity (Guo et al., 2013; Kalashnikova et al., 2013). In particular, we used the daily dark-water non-spherical AOD retrieval (at 557.5 nm) provided by the MISR Level 3 Component Global Aerosol Product (MIL3DAE, Version F15\_0031) dataset, on a  $0.5^\circ \times 0.5^\circ$  spatial grids during the period 2000–2016.

However, we should note here that the dark-water retrieval sensitivity to particle non-sphericity decreases when the total AOD is below about 0.1 and when the non-spherical component contributes less than 15–20 % to the total AOD (Kalashnikova and Kahn, 2006; Pierce et al., 2010; Kalashnikova et al., 2013). As a result, non-spherical particles are sometimes retrieved over remote oceans, even where they are unlikely to be present, overestimating non-spherical AOD fraction, probably due to the presence of unscreened cirrus or other naturally occurring non-spherical aerosols (Pierce et al., 2010; Kalashnikova et al., 2013; Kahn and Gaitley, 2015). On the other hand, the dark-water non-spherical AOD retrieval performs quite well in regions of dust transport where the AOD values are significant and the non-spherical component is dominant. As previous studies have shown (Kalashnikova and Kahn, 2006, 2008), this is especially true over the Tropical Atlantic where desert dust is the dominant aerosol component, accounting for 40–70 % of the total AOD (Guo et al., 2013).

The spatial collocation between the two datasets was obtained by re-gridding MONARCH DOD, using the coarser MISR Level 3 product grid as a reference. For the temporal collocation we followed a similar methodology as in the case of MIDAS: MISR on board of NASA's Terra satellite is crossing the equator on the descending node at about 10:30 LT. ~~After having converted 10:30 LT to UTC time taking into account the related longitude, the and the~~ MONARCH DOD was temporally averaged around MISR overpass time using the two nearest MONARCH timeslots. MISR has only 1/4 to 1/3 the spatial sampling of MODIS due to its relatively narrow swath width ( $\sim 380$  km), resulting in global coverage every 7–9 days at mid-



to-low latitudes, compared with 1–2 days by MODIS. So, sampling must be taken into consideration when comparing datasets  
235 averaged over longer timescales.

## 2.4 IASI dust product: AEROIASI

The Infrared Atmospheric Sounding Interferometer (IASI) instrument is in orbit onboard EUMETSAT’s MetOp satellite, providing temperature and water vapor profiles of the troposphere and lower stratosphere at vertical and horizontal resolutions of 1 km and 12 km, respectively. IASI measurements in the infrared part of the electromagnetic spectrum enable observations  
240 both in daytime and nighttime conditions. Thanks to its wide swath (2200 km), IASI provides global coverage twice a day, crossing the equator on the descending node at approximately 09:30 and 21:30 LT. Desert dust profiles can be derived from individual thermal infrared spectra measured by IASI for most cloud-free IASI pixels, both over land and ocean, following the method called AEROIASI, developed by Cuesta et al. (2015). Information on the vertical distribution of dust is provided mainly by their broadband radiative effect, which includes aerosol thermal emission depending at each altitude on the vertical  
245 profile of temperature. [AEROIASI](#) Unlike most IASI dust products (e.g., Clarisse et al., 2019), the AEROIASI dataset provides both vertical and column-integrated dust extinction information. More specifically, AEROIASI products include twice-daily 3D distributions of dust extinction coefficient, although the present study only uses dust horizontal distributions derived in terms of DOD.

The AEROIASI algorithm firstly uses as input a priori dust microphysical properties (e.g., a dust number concentration  
250 profile as well as its size distribution and complex refractive index) and meteorological variables (temperature profiles, surface temperatures and H<sub>2</sub>O profiles) to simulate thermal infrared radiance spectra, which are then compared to those measured by IASI. In order to fit IASI observations and to minimize the spectral residuals, the method iteratively adjusts the radiative transfer inputs, namely the dust profile and surface temperature, using Tikhonov–Philips-type regularization, until reaching good agreement for different atmospheric and surface conditions. The a priori dust profile used in every pixel (the same profile  
255 for all pixels and all seasons) is a first guess of dust vertical distribution obtained from an average of dust extinction vertical profiles over the Sahara Desert, retrieved from CALIPSO/CALIOP satellite observations (Winker et al., 2009). Once IASI spectra are fitted, a series of quality checks is performed to screen out cloudy measurements and aberrant retrievals, even though sub-visible cirrus clouds (with AOD below  $\sim 0.02$ ) may be difficult to screen out. Then, the final outputs of AEROIASI are calculated for each unscreened pixel, providing a vertical profile of dust extinction coefficient at 10  $\mu\text{m}$  and the associated  
260 DOD by vertical integration of the extinction profile. Using thermal infrared measurements, AEROIASI retrievals are mostly sensitive to coarse aerosols (with a radius roughly greater than  $\sim 2$ ). In fact, the contribution of [fine dust particles to total DOD](#) finer dust particles (with radii  $< \sim 1$   $\mu\text{m}$ ) to total AOD at 10  $\mu\text{m}$  is expected to be less than  $\sim 10$  % (Pierangelo et al., 2005); consequently, the AEROIASI product considered here is the coarse mode DOD at 10  $\mu\text{m}$ . The AEROIASI retrieval offers different sensitivities over land and the ocean. Normally, there is more sensitivity over land, as the surface temperature deviates  
265 more from that of the atmosphere above as compared to the case over the ocean. However, the surface emissivity over land is less well known and might induce local biases. Moreover, comparisons conducted between AEROIASI and AERONET coarse AOD retrievals showed distinct discrepancies between the two datasets in many sites over and downwind of the Sahara Desert

(Cuesta et al., 2020) and AEROIASI overestimations far away from desert dust sources (Cuesta et al., 2015). The biases in both cases reach or even exceed 0.1 in absolute value. Additionally, the use of non-zero a priori values for dust abundance (equivalent to an AOD at 10  $\mu\text{m}$  of  $\sim 0.03$ ) is expected to induce positive biases in situations with both very low dust abundances and low sensitivities, as encountered for the relatively lower surface temperatures of mid-latitudes as compared to those near the tropics. Developments for future versions of the product will aim at screening out these low sensitivity situations.

In this study, we used coarse DOD over the period 2008–2016, provided by the AEROIASI Version 3 dataset, which was retrieved from MetOp-A/IASI data (IASI-A, Level 3), whose mission was completed in November 2021. The horizontal resolution of the AEROIASI dataset is  $1^\circ \times 1^\circ$ . The DOD at 10  $\mu\text{m}$  was obtained by vertically integrating the extinction coefficient and then it was spectrally converted from 10  $\mu\text{m}$  to 550 nm using a conversion factor of 1.70, derived with a Mie code. The derived AEROIASI coarse DOD (at 550 nm) considers coarse dust particles larger than 0.6  $\mu\text{m}$  in radius. The spatial collocation between the two datasets was achieved by re-gridding MONARCH coarse DOD through bilinear interpolation using the coarser AEROIASI grid as a reference. Finally, MONARCH was linearly interpolated in terms of time over the exact date-time of the IASI retrievals, as provided by the AEROIASI dataset.

## 2.5 AERONET dust-filtered products

High-quality aerosol optical properties are provided by the ground-based photometer network of AERONET RObotic NETwork (AERONET; Holben et al., 1998; O’Neill et al., 2003; Giles et al., 2019). These instruments rely on extinction measurements of the direct and scattered solar radiation at several nominal wavelengths (between 340 and 1020 nm). In addition, direct-sun AOD processing includes the Spectral Deconvolution Algorithm (SDA) described in O’Neill et al. (2003). This algorithm yields submicron (fine) and super-micron (coarse) AOD at a standard wavelength of 500 nm from which the fraction of fine mode to total AOD can be computed. The algorithm fundamentally depends on the assumption that the coarse mode Ångström exponent and its derivative are close to zero. AERONET provides a long-term and continuous database of aerosol optical, microphysical and radiative properties, the best currently available on a global basis for aerosol research and characterization, validation of satellite retrievals and evaluation of aerosol models.

~~The descriptions of the MIDAS, MISR, and AEROIASI dust products above summarized the features and the uncertainties of the total and coarse DOD products which depend upon the instruments’ capabilities, the limitations of the retrieval techniques, and the validity of the assumptions made in order to separate mineral dust aerosols from other aerosol components. All four observational datasets (including AERONET) have their advantages and disadvantages, thus can be complementary to each other in order to overcome limitations regarding the quality of the dust retrievals and the spatiotemporal coverage: MIDAS provides total and coarse DOD observations both over land and sea with the finest spatial resolution ( $0.1^\circ \times 0.1^\circ$ ); MISR provides the most physically robust separation of DOD by discriminating dust aerosols based on actual retrieved particle shape information; AEROIASI has the most frequent sampling, covering the Earth twice a day, and it is the only dataset to provide nighttime measurements; AERONET ground-based measurements provide the finest temporal resolution ( $\sim 15$  minutes), giving the possibility to assess MONARCH at its original 3-hourly time scale. Moreover, the signal-to-noise ratio for the AERONET direct-sun measurements is high and the surrounding surface reflectance usually makes no significant~~

~~contribution to the signal in most cases. This renders AERONET AOD the best available source for surface-based particle property retrieval results, therefore in this study the AERONET dust-filtered retrievals were used not only to assess the model outputs but also to validate the quality of the satellite-based dust products (see Sect. 3).~~

305 In this study, we used AERONET Version 3 quality-assured data (i.e., Level 2.0) as a reference dataset (Giles et al., 2019). Since AOD includes contributions from different types of particles, a dust-filter method was applied to identify AOD observations in which dust is the dominant aerosol type. AERONET dust-filtered AOD (i.e., DOD) is based on direct-sun AOD retrievals between 440 and 870 nm. Although direct-sun does not yield AOD at 550 nm, this variable is calculated from the AOD at 440, 675 and 870 nm and the Ångström Exponent at 440–870 nm (AE) using the Ångström’s law. Then AE is used  
310 as a filter because it is inversely related to the average aerosol size. Lower AE values ( $< 1$ ) indicate significant presence of coarse-mode particles (e.g., mineral dust and sea-salt), whereas higher AE values ( $> 1$ ) values imply a large abundance of fine particles (e.g., biomass burning and urban aerosols; Papagiannopoulos et al., 2018). Here we follow the discrimination method of Basart et al. (2009), where DOD = AOD when  $AE < 0.75$ , and all data with  $AE > 1.2$  are considered free of dust, i.e., DOD = 0. These two definitions can introduce uncertainties, and in particular, a potential over- and underestimation of the total dust  
315 contribution, respectively. Other studies have used lower discrimination thresholds (e.g.,  $AE < 0.6$ ), in an effort to obtain pure mineral dust conditions (e.g., Di Tomaso et al., 2022), but thereby excluding more AOD observations in long-range transport regions. Finally, ~~in this study~~ a mixed aerosol type is assumed when  $0.75 \leq AE \leq 1.2$  and ~~the corresponding AOD values are not considered for our analysis~~ since we cannot precisely estimate the contribution of dust to it, these cases are not used for the evaluation purposes of this study.

320 Regarding AERONET coarse AOD, it was retrieved based on the SDA which yields fine and coarse mode AOD at 500 nm, assuming particle radius  $0.6 \mu\text{m}$  as the inflection point in the volume size distribution. The coarse mode AOD is dominated by maritime/oceanic aerosols and desert dust, whereas other natural sources, such as wildfires, can also produce coarse-mode aerosols. Sea-salt is usually associated with low AOD ( ~~$\ll 0.03$ ; Dubovik et al., 2002~~) ( $< 0.03$ ) and mainly affects coastal stations, and therefore inland high coarse AOD values is assumed to be mineral dust, although significantly high AOD values  
325 could be associated with biomass burning particles because they are more absorbing than dust (Dubovik et al., 2002). Moreover, any disparity between the wavelength difference 550 nm and 500 nm is negligible, as coarse mineral dust is wavelength-independent in the visible range (Eck et al., 1999). Therefore, coarse AOD from AERONET SDA will be used as the corresponding AERONET coarse DOD.

Both AERONET dust-filtered retrievals (total and coarse DOD) are dominated by mineral dust; however, small-size particles  
330 (anthropogenic aerosols, biomass burning, etc.) are always present, especially far away from the sources, whereas sea-salt particles can contaminate our retrievals mainly at AERONET stations close to the coast (Basart et al., 2009). Moreover, AERONET particle properties retrieved from sky-scan measurements (e.g., coarse AOD), can be contaminated by the reflectance of the various surface types, such as snow, ice or even some desert surfaces (Sinyuk et al., 2007). Consequently, an overestimate of the AERONET total and coarse DOD is expected.

335 All the AERONET stations located within the MONARCH reanalysis geographical domain and operating during the reanalysis period were considered, excluding the stations that are at high altitudes ( $> 2$  km above sea level). ~~In total,~~ Overall, total

and coarse DOD retrievals from 238 stations were used for the present analysis. ~~Total and coarse DOD datasets from the dust regional reanalysis were bilinearly interpolated.~~ The two datasets were spatially collocated by interpolating MONARCH over each AERONET station. Regarding the temporal collocation, AERONET data are acquired at 15-minute intervals on average; therefore, all AERONET measurements within  $\pm 90$  minutes of the ~~model-~~MONARCH reanalysis outputs have been averaged for the comparison on a 3-hourly basis. Figure 2-4u shows the location of the AERONET sites with at least 30 temporally collocated pairs available (224 in total).

The descriptions of the MIDAS, MISR, AEROIASI and AERONET dust products above summarized the features and the uncertainties of the total and coarse DOD products which depend upon the instruments' capabilities, the limitations of the retrieval techniques, and the validity of the assumptions made in order to separate mineral dust aerosols from other aerosol components. All four observational datasets have their advantages and disadvantages, thus can be complementary to each other in order to overcome limitations regarding the quality of the dust retrievals and the spatiotemporal coverage: MIDAS provides total and coarse DOD observations both over land and sea with the finest spatial resolution ( $0.1^\circ \times 0.1^\circ$ ); MISR provides the most physically robust separation of DOD by discriminating dust aerosols based on actual retrieved particle shape information; AEROIASI has the most frequent sampling, covering the Earth twice a day, and it is the only dataset to provide nighttime measurements; AERONET ground-based measurements provide the finest temporal resolution ( $\sim 15$  minutes), giving the possibility to assess the MONARCH reanalysis at its original 3-hourly time-scale. Moreover, the signal-to-noise ratio for the AERONET direct-sun measurements is high and the surrounding surface reflectance makes no significant contribution to the signal in most cases. This renders AERONET AOD the best available source for surface-based particle property retrieval results, therefore in this study the AERONET dust-filtered retrievals were used not only to assess the MONARCH reanalysis outputs but also to validate the quality of the satellite-based dust products (see Sect. 3).

## 2.6 Evaluation strategy

The evaluation metrics that were used to quantify the level of agreement between the ~~model-~~MONARCH reanalysis simulations and the observations are the mean bias (MB), the root mean square error (RMSE), the fractional gross error (FGE) and the correlation coefficient (CC), the definitions of which are given in Appendix A.

The inter-comparison of total and coarse DOD was conducted over two different temporal scales (annual and seasonal) and over two different spatial scales (grid-point and regional). All the statistical indicators (Table A1) were computed on an annual scale, considering all the different ~~model-~~MONARCH and satellite datasets collocated pairs for the period 2007–2016 of the reanalysis, and on a seasonal scale where the collocated data of a certain season were compared throughout the years according to the following classification: boreal winter (December-January-February: DJF), boreal spring (March-April-May: MAM), boreal summer (June-July-August: JJA) and boreal autumn (September-October-November: SON). The seasonal subdivision of the datasets allows for the assessment of the MONARCH reanalysis performance in reproducing the annual cycle and the seasonal patterns of the total and coarse DOD. The aforementioned temporal aggregations were generated for each grid-point of the reanalysis-satellite collocated data and for each individual AERONET station.

370 Moreover, the evaluation statistics were produced at a regional scale in order to assess ~~model performance~~ [the MONARCH reanalysis](#) over regions with distinct characteristics. The study geographical domain has been divided in ten specific sub-regions (Fig. 1) where the ~~model~~ scores were computed considering all the ~~modelled reanalysis~~ and satellite-based dust product pairs contained in each one of them, giving the opportunity to identify any dependencies between the different ~~model~~ [MONARCH](#) and satellite datasets and the features of each region. The ten sub-regions are mainly classified into three groups: (i) continental  
375 regions that contain the mineral dust sources, where high DOD is observed throughout the year: Northern Africa, Middle East and Western Asia (hereafter NorAfr, MidEas and WesAsi, respectively); (ii) remote regions of rare dust events, suitable for [the MONARCH](#) reanalysis evaluation under conditions of very low DOD: North Atlantic, ~~Northern~~ [North-Central](#) Europe and Russia (hereafter NorAtl, NorEur and Russia); (iii) maritime and continental regions located downwind of the dust sources, which contain the main dust transport pathways: Tropical Atlantic, Mediterranean Sea, Arabian Sea and Sub-Saharan Africa  
380 (hereafter TroAtl, MedSea, AraSea and SubSah). The latter are subject to seasonal DOD variation. Furthermore, the borders between the regions are defined so that every region consists mainly of one surface type (i.e., land or sea). This rough approximation can improve the interpretation of the regional results, considering that the surface type is associated with the retrieval algorithms used to derive AOD from the satellite observations.

~~Nevertheless, differences between the inter-comparison results obtained from the different datasets do exist in some cases. These discrepancies may be due to several possible reasons related to the features of the datasets and the region. The uncertainties involved in the derivation of MIDAS, MISR, AEROIASI, and AERONET dust products inevitably contribute to their differences too. All satellite-based instruments have increased difficulty retrieving particle properties at low AOD—let alone the DOD fraction in regions where it is even lower—especially over some surface types for which the reflectance can negatively impact the retrieval quality. AERONET’s discrimination method can also allow large sea salt particles to be misclassified as dust, especially at coastal sites. Moreover, MISR has much less frequent sampling compared to MIDAS, whereas AERONET’s fine temporal resolution permits the detection of sub-daily micro- and mesoscale dust activity caused by local sources, that satellites’ less frequent sampling can miss. Lastly, unfavorable observing conditions, such as cloud cover common at high latitudes especially during wintertime, in addition to basic sampling frequency, can also decrease the quality of DOD retrievals, for example due to unmasked cirrus clouds misclassified as dust.~~

395 ~~Finally, Lastly,~~ a multi-sensor aggregation comparison [at a regional scale](#) based on the considered satellite-based ~~dust DOD~~ datasets (i.e., MIDAS, MISR and AEROIASI) is applied to get an overall assessment of the [MONARCH performance reanalysis](#). We excluded AERONET from the multi-sensor aggregation ~~at a regional scale~~ because the representativeness of the computed regional metrics remains questionable due to the uneven distribution of stations in the various sub-regions both quantitatively and spatially (Fig. 2, 2). For example, a large number of network sites sufficiently covers the Mediterranean region and ~~Northern~~  
400 [North-Central](#) Europe, whereas only one station corresponds to the Arabian Sea, which is additionally located at the edge of the sub-region.

The regional evaluation metrics of each satellite dataset were averaged to one final value weighted by the number of the ~~model~~ [MONARCH reanalysis](#) and satellite-based dust product pairs that each dataset contributes within each sub-region. Even though we consider the contributions of all the available collocated pairs, it is noted that the different sampling frequencies

405 (temporal resolution) and overpass times for a given location of the satellites considered in the study, complement each other, providing together higher temporal coverage. The weighted mean of the statistical indicators was computed at annual and seasonal scale for every sub-region according to the equations shown in Table A2.

410 The next two sections present the results of the MONARCH reanalysis assessment as well as the validation of the satellite datasets using ground-based measurements. An overview of the datasets evaluated and the datasets used as reference, of the spatial and temporal scales at which the evaluation was performed, and of the figures that depict the results is outlined in Table 1 to help the reader navigate between the following sections.

**Table 1.** Index of the datasets assessed in Sect. 3 and 4.

|  | <u>Evaluated datasets</u>                             | <u>Reference datasets</u>  | <u>Spatial scale</u>                | <u>Temporal scale</u>             | <u>Section</u>                    | <u>Figure</u>         |
|--|---|--|-------------------------------------|-----------------------------------|-----------------------------------|-----------------------|
| <u>Validation of satellite dust products</u> | <u>MIDAS DOD</u><br><u>MISR DOD</u>                   | <u>AERONET DOD</u>   | <u>Station</u>                      | <u>Annual</u>                     | <u>3.1</u>                        | <u>2</u>              |
|  | <u>MIDAS coarse DOD</u><br><u>AEROIASI coarse DOD</u> | <u>AERONET coarse DOD</u>  | <u>Station</u>                      | <u>Annual</u>                     | <u>3.2</u>                        | <u>3</u>              |
| <u>MONARCH reanalysis assessment</u>         | <u>MONARCH DOD</u>                                    | <u>MIDAS DOD</u><br><u>MISR DOD</u><br><u>AERONET DOD</u>                          | <u>Grid-point</u><br><u>Station</u> | <u>Annual</u>                     | <u>4.1.1</u>                      | <u>4</u>              |
|  |   |  | <u>Regional</u>                     | <u>Annual</u><br><u>Seasonal</u>  | <u>Supplement</u>                 | <u>S1; S2; S3</u>     |
|  |   | <u>MIDAS+MISR DOD</u>  | <u>Regional</u>                     | <u>Annual</u><br><u>Seasonal</u>  | <u>4.2.1</u><br><u>Supplement</u> | <u>6</u><br><u>S4</u> |
|  | <u>MONARCH coarse DOD</u>                             | <u>MIDAS coarse DOD</u><br><u>AEROIASI coarse DOD</u><br><u>AERONET coarse DOD</u> | <u>Grid-point</u><br><u>Station</u> | <u>Annual</u>                     | <u>4.1.2</u>                      | <u>5</u>              |
|  |   |  | <u>Regional</u>                     | <u>Annual</u><br><u>Seasonal</u>  | <u>Supplement</u>                 | <u>S5; S6; S7</u>     |
|  | <u>MIDAS+IASI coarse DOD</u>                          | <u>Regional</u>  | <u>Annual</u><br><u>Seasonal</u>    | <u>4.2.2</u><br><u>Supplement</u> | <u>7</u><br><u>S8</u>             |                       |

### 3 Satellite-derived dust products inter-comparison with AERONET

A robust ~~model~~-reanalysis assessment requires the observational data to be reliable and consistent across the study spatial domain, regardless of surface type and the intensity of dust activity. The uncertainties that satellite data can present under certain conditions, as described earlier in Sect. 2, are likely to skew the results of the ~~model~~-MONARCH reanalysis assessment. In order to identify the main performance skill of the satellite-derived dust data, in this section we perform a quality check based on comparisons with ground-based AERONET observations. AERONET data have already been used as a “gold standard” for validating most satellite AOD products. Although MIDAS, MIRS and AEROIASI have been evaluated using dust-related AERONET retrievals in independent analysis (Gkikas et al., 2021; Kahn and Gaitley, 2015; Kalashnikova and Kahn, 2006; Cuesta et al., 2015, 2020), here we seek to assess the performance of the different satellite-based dust products in a common framework (spatial and temporal) for the later comparison with the ~~dust~~-MONARCH reanalysis.



The comparison between satellite-based dust products and AERONET is performed for each station individually using collocated satellite and ground-based measurements. Each satellite dataset was spatially averaged over the AERONET sites, and the AERONET time-series were temporally averaged centered on the satellite overpass time at the site. The criteria of spatiotemporal coincidence are  $\pm 2$  hours for AERONET and  $\pm 1^\circ$  of latitude and longitude for AEROIASI,  $\pm 0.5^\circ$  for MISR and  $\pm 0.2^\circ$  for MIDAS, according to the spatial resolution of each satellite dataset used. The time-series that emerged from the collocation were then compared to each other using the metrics defined in Table A1. In addition, DOD time-series retrieved from MIDAS and MISR (hereafter MIDAS+MISR), as well as coarse DOD retrievals from MIDAS and AEROIASI (hereafter MIDAS+IASI), were combined at station level and then compared to AERONET with the aim to investigate if an aggregated satellite multi-sensor product could statistically mitigate the weaknesses of each sensor and the biased values they introduce into the individual products.

### 3.1 MIDAS and MISR DOD compared to AERONET

Figure 2 shows the DOD comparison of the satellite MIDAS (Fig. 2, 1<sup>st</sup> column), MISR (Fig. 2, 2<sup>nd</sup> column) and MIDAS+MISR (Fig. 2, 3<sup>rd</sup> column) dust products with AERONET observations. As it is expected, overall all annual DOD values (Fig. 2a–f) shows a marked south-to-north gradient with DODs maxima (above 0.36) in the Sahel (Fig. 1, “D”) and the Middle East (latitudes  $< 30^\circ$  N) and DOD minima in continental Europe and Russia (under 0.05). The CC between MIDAS and MISR against AERONET (Fig. 2p–q) is very high at all stations affected by dust regularly (CC  $> 0.8$ ), whereas it drops below 0.4 at sites where the presence of dust is less frequent, reaching even negative values, down to  $-0.4$ , at few coastal stations of Northern-northern Europe.

The DOD comparison of MIDAS and MISR against AERONET shows underestimations (MB  $< 0$ ) at most sites situated close to or around the dust sources in Northern Africa and the Middle East and slight overestimations in Europe (MB up to 0.04). In particular, MIDAS largest underestimations (MB  $< -0.1$ ) are recorded at stations located along with the dust outflow from the Sahara Desert to the Gulf of Guinea and the Atlantic Ocean, in agreement with Gkikas et al. (2021) and Wei et al. (2019), as well as at some stations in the Arabian Peninsula and Western Asia on the coastline with the Arabian Sea (Fig. 2g). At stations located in the western Sahara Desert and the western part of the Sahelian Belt MIDAS shows low RMSE (up to 0.12) As in the case of MB, MIDAS presents maximum RMSE near to the coasts of the Gulf of Guinea ( $> 0.32$ ; Fig. 2j) and FGE (up to 0.7; Fig. 2m); however, RMSE is relatively low ( $< 0.24$ ) along the Sahelian Belt and across the Arabian Peninsula, considering the high DOD values (annual DOD mean above 0.36 for both MIDAS and AERONET).

Similarly, MISR presents overall underestimation (MB  $> 0.32$ ) observed there by both AERONET and MIDAS. This also applies to MIDAS FGE that remains low ( $< 0.7$ ) in regions of high dust activity (Fig. 2m).

MISR MB shows an overall underestimation at the majority of the AERONET sites, which exceeds  $-0.07$ ), particularly at all the stations along the coastlines of Africa and the Middle East (in the surroundings of the dust sources. The largest underestimations can be found along the Northern Africa coastline and in the Red Sea, where MB  $< -0.1$ ) (Fig. 2h). In the Mediterranean Sea and continental Europe, MISR shows smaller differences against AERONET associated with the lower

455 DODs in these long-range transport regions (annual DOD mean up to 0.09 for MISR and AERONET) with RMSE up to 0.08  
(Fig. 2k), MB ranges between  $-0.04$  and  $0.04$  and FGE achieving maximum values (up to 2; Fig. 2n).

Lastly, the combination of MIDAS and MISR DOD at station level into a single time series (i.e., MIDAS+MISR) compared  
to AERONET do not show major deviations with respect to the independent MIDAS and MISR datasets, and at most sites  
they are identical to MIDAS scores. This is due to the fact that MISR contributes to less than 40 % of the 238 available sites  
460 and that is only at coastal stations. Moreover, the impact of each sensor to the final product is determined by the number  
of measurements available at each station (Fig. 2s–t), where in most sites MIDAS exceeds MISR sampling in number N of  
observations, due to its higher temporal resolution.

### 3.2 MIDAS and AEROIASI coarse DOD compared to AERONET

The coarse DOD comparison with MIDAS and AEROIASI against AERONET (Fig. 3) shows different results. As expected,  
465 overall annual coarse DOD values (Fig. 3a–f) show a marked south-to-north gradient with DODs maxima in the Arabian  
Peninsula ( $> 0.23$  for both sensors) and in the Sahel ( $> 0.27$  for MIDAS and no more than  $0.23$  for AEROIASI) and DOD  
minima in continental Europe and Russia ( $< 0.05$  for MIDAS but no less than  $0.09$  for AEROIASI). The MIDAS CC map  
shows a very clear correlation ( $CC > 0.8$ ) with AERONET coarse DOD over all the dust source regions and the Mediterranean  
Sea, and a fairly high correlation ( $CC > 0.6$ ) at most sites in Northern-North-Central Europe (Fig. 3p). On the other hand,  
470 AEROIASI CC ranges between  $0.4$  and  $0.8$  at AERONET sites located up to  $40^\circ$  N, whereas no correlation ( $CC \sim 0$ ) or even  
negative correlation was computed at all sites across Northern-North-Central Europe and Russia (Fig. 3q), showing significant  
weakness in reproducing the temporal evolution of coarse DOD in those regions. Similar tendencies are found for RMSE (Fig.  
3j–k) and FGE (Fig. 3m–n) between the two satellite-derived dust products; however, AEROIASI provides relatively greater  
errors compared to MIDAS, at almost all AERONET stations, and for both metrics, something that affects the multi-sensor  
475 product as well, especially in northern latitudes (Fig. 3l and o).

Overall, MIDAS underestimates the coarse DOD compared to AERONET (MB ranges from  $0.01$  in Europe to less than  $-0.1$   
in the Sahel; Fig. 3g) whereas AEROIASI shows overestimations (MB  $> 0.04$ ) almost everywhere except for the Sahel, Gulf  
of Guinea, Capo Verde and the Persian Gulf (MB  $< -0.04$ ; Fig. 3h). The results of MIDAS coarse DOD in Europe (with MB  
 $< 0$ ; Fig. 3g) with respect to MIDAS total DOD results (with MB  $> 0$ ; Fig. 2g) emphasizes the fact that the size distribution of  
480 MIDAS is skewed toward finer fractions. This is directly connected with the use of the MERRA-2 reanalysis fine/coarse DOD  
ratio for the MIDAS total and coarse DOD estimations (see Sect. 2.2). As pointed out by Buchard et al. (2017), MERRA-2  
shows a larger contribution of dust fine fractions to the total dust budget. Regarding AEROIASI, MB results (Fig. 3h) are  
consistent with the findings of previous studies, namely MB ranges from  $-0.1$  to  $0.1$  over the Sahara Desert (Cuesta et al.,  
2020) and overestimation of coarse DOD reaches  $0.1$  far from the desert dust sources (Cuesta et al., 2015). Positive biases  
485 encountered north of  $40^\circ$  N are most likely linked to the use of non-zero a priori values for the retrieval. When the abundance  
of dust and the product sensitivity too are low (as frequently expected north of  $40^\circ$  N), the Tikhonov–Philips inversion used by  
AEROIASI tends to provide the a priori value which are clearly visible in terms of long-term averages (as in the case of Fig.  
3).

The MIDAS+IASI product was derived from the aggregation of the two datasets (Fig. 3e3c), to which they contribute  
490 equally at stations located at lower latitudes, whereas AEROIASI's impact is bigger at sites in ~~Northern~~ North-Central Europe  
and Russia, owing to the higher number of IASI measurements available in those regions (Fig. 3s–u). MIDAS+IASI CC  
(Fig. 3r) provides low correlation (CC < 0.2) at all AERONET stations in ~~Northern~~ continental Europe (latitudes > 45° N).  
MIDAS+IASI shows strong underestimation (MB < -0.1) in the southwest of the Sahara Desert and on the coast of Pakistan,  
whereas overestimation is observed in Morocco (MB > 0.1) and Europe (MB up to 0.07 in northern latitudes; Fig. 3i). These  
495 overestimates in Europe are directly associated with the strong overestimations of AEROIASI (Fig. 3h). MIDAS+IASI is in  
good agreement with coarse DOD AERONET along the northern coast of Africa and the Red Sea, and in most sites across the  
Mediterranean Sea (-0.01 < MB < 0.01). As a result, the MIDAS+IASI coarse DOD product is more reliable over dust-rich  
regions and becomes more uncertain in regions of sporadic dust events, although, overall its performance is poorer than the  
only-MIDAS' coarse DOD.

## 500 4 MONARCH reanalysis assessment

In this section the assessment of total DOD and coarse DOD products of the MONARCH reanalysis for 2007–2016 is an-  
alyzed. Firstly, MONARCH is compared versus each observational-based dust dataset (i.e., AERONET, MIDAS, MISR and  
AEROIASI) at station level in the case of AERONET and at grid-cell level considering the individual grids for each satellite  
dataset. Then, the comparison was made at regional scale by generalizing the results based on the ten sub-regions shown in  
505 Fig. 1. The regional scores were computed at two different temporal scales as well: annual and seasonal. Finally, an overall  
assessment is attempted through the aggregation of the regional results that were obtained by the evaluation against the satellite  
datasets.

### 4.1 Independent dataset analysis

#### 4.1.1 MONARCH DOD compared to MIDAS, MISR and AERONET

510 Starting with the MONARCH DOD assessment, Fig. 4 shows the results of the comparison with DOD products retrieved from  
the space-based and ground-based observations. At first glance, MONARCH seems to capture the DOD spatial distribution  
obtained by the all three observational datasets (i.e., MIDAS, MISR and AERONET), reproducing the major dust hotspots and  
the dust transport pathways in the area (Fig. 4a, e and e4a–c). More specifically, ~~the reanalysis~~ MONARCH DOD exceeds 0.27  
over all the dust sources listed in Fig. 1, with values exceeding 0.36 over the western Sahara Desert, the Bodélé Depression  
515 (Fig. 1, “E”), the Sahel and the Arabian Peninsula (Fig. 4a and ec). Moreover, a pronounced dust plume is simulated stretching  
across the Tropical Atlantic Ocean. The magnitude and latitudinal extent are greatest over the west African coastline with the  
maximum DOD up to 0.32 and gradually decreasing westward towards the central Tropical Atlantic, as expected for a dust  
plume that originates in Africa. Similarly, moderate dust transport is simulated over the adjacent regions of the Mediterranean

and the Arabian Sea with maximum DOD values up to 0.18 and 0.23 respectively, closer to the dust sources (Fig. 4a and 4b).

The comparison between MONARCH and MIDAS shows a strong correlation over the entire domain, with CC maxima ( $> 0.8$ ) found throughout the Sahara Desert, the Sahel Belt, the Middle East and the Tropical Atlantic and partially over the Arabian Sea, the Mediterranean Sea and even in the North Atlantic (Fig. 4p). The correlation between reanalysis-MONARCH and MISR DOD (Fig. 4q) is higher ( $CC > 0.6$ ) around the dust source areas but is poorer over the North Atlantic, reaching zero or negative values, presumably associated with MISR's limited sampling compared to MIDAS (Fig. 4s-t). The reanalysis MONARCH DOD is highly correlated with AERONET observations over sites affected by medium-range dust transport, whereas the CC diminishes ( $< 0.4$ ) towards the northern latitudes of the study region, especially close to coastal areas (Fig. 4r), where the number of observations used for the comparison is  $< 250$  (Fig. 4u). Furthermore, RMSE (Fig. 4j-l) and FGE (Fig. 4m-o) spatial distributions are similar in the comparison of the reanalysis-MONARCH DOD with MIDAS, MISR and AERONET, showing maximum RMSE values ( $> 0.24$ ) and minimum FGE values ( $\sim 0$ ) in the regions more affected by the presence of mineral dust with high DOD ( $> 0.18$  on annual average), as well as minimum RMSE values ( $\sim 0$ ) and maximum FGE values ( $\sim 2$ ) in the long-range transport regions (annual DOD  $< 0.05$ ).

Overall, the MONARCH reanalysis tends to underestimate DOD except in desert dust source regions where MONARCH the reanalysis and the observational datasets show some discrepancies. In the comparison with MIDAS reveals a strong MB discontinuity from land to sea and especially from the dust sources to the adjacent maritime regions (Fig. 4g), the. In particular, the MONARCH reanalysis shows overall overestimations in Northern Africa, the Arabian Peninsula and the part of Kazajistan, Uzbekistan and Turkmenistan with larger overestimation ( $MB > 0.1$ ) in the dust sources of Algeria, over the Sahel, the Bodélé Depression and the Ustyurt Plateau (Fig. 1, "A", "B", "D", "E" and "J") and underestimation ( $MB < 0$ ) in the Persian Gulf and the arid regions of Iran and Afghanistan (Fig. 1, "K"). Regarding the comparison with AERONET (Fig. 4i), MONARCH the MONARCH reanalysis presents an overall underestimation, with  $MB < -0.1$  in western part of the Sahel and near to the coast of the Gulf of Guinea, except in the downwind sites of the Bodélé Depression and over the Great Sand Sea (Fig. 1, "F") where maximum overestimations ( $MB > 0.1$ ) are observed. Over continental Europe and Russia, near-zero MB is observed compared to both datasets, because of the relatively lower DOD by MIDAS and AERONET and simulated by MONARCH in those regions. Over the maritime regions, the comparison with MIDAS, MISR and AERONET shows similar results. The MONARCH reanalysis strongly underestimates the dust transport towards the Gulf of Guinea and in Cape Verde ( $MB < -0.1$ ), whereas it moderately underestimates (down to  $-0.07$ ) and overestimates (up to  $0.04$ ) over the Tropical Atlantic and the central and eastern Mediterranean Sea, respectively. Particularly over the North Atlantic and the Arabian Sea, the comparison of MONARCH with MISR shows higher RMSE values (up to  $0.16$ ; Fig. 4k) and larger underestimations ( $-0.04 < MB < -0.07$ ; Fig. 4h) compared to MIDAS ( $-0.01 < MB < -0.04$ ; Fig. 4g), because of the relatively higher DOD recorded by MISR in these regions (Fig. 4d4e). This difference between MISR and MIDAS DOD can be traced to the difference between MISR and MODIS total AOD, as in previous studies MISR AOD was found to be generally larger than MODIS AOD over water (Guo et al., 2013; Abdou et al., 2005; Kahn et al., 2010).

The comparison of MONARCH DOD with each observational dataset was made at regional level as well, based on the ten sub-regions shown in Fig. 1. The statistical parameters were computed at regional scale and at two different temporal scales, annual and seasonal, and are presented in Supplement. In particular, the regional results of the MONARCH comparison against MIDAS, MISR and AERONET are shown in Fig. S1, Fig. S2 and Fig. S3, respectively. The seasonal and regional DOD patterns show good agreement between MONARCH and MIDAS (Fig. S1), identifying MAM and JJA as the seasons of maximum dust emissions from the sources ( $DOD > 0.3$  in NorAfr and MidEas). In MAM the meteorological conditions favor the transport of dust from the southern parts of the Sahara (e.g., Bodélé Depression) to the Sahel (~~DOD ~ 0.3 in SubSah~~)(DOD ~ 0.3 in SubSah; Kaly et al., 2015), and from the northern Sahara sources and the Syrian Desert (Fig. 1, “G”) towards the Mediterranean (Solomos et al., 2018). In JJA dust plumes are directed from the Sahara and the Middle East towards the Atlantic and the Arabian Sea, respectively. This dust transport seasonality is also confirmed by the seasonal values of MONARCH and MISR over the maritime regions (Fig. S2), which are fully covered by MISR dark-water retrievals. On the other hand, the low sensitivity of MISR non-spherical AOD over the remote regions (NorAtl, NorEur and Russia) is evident here, leading to overestimated annual and seasonal MISR DOD values (annual  $DOD > 0.05$ ), higher biases (annual  $MB < -0.05$  and  $RMSE > 0.09$ ) and lower  $CC (< 0.21)$  with MONARCH. Lastly, the regional means obtained from MONARCH versus AERONET comparison (Fig. S3) should be used with caution because the sub-regions are not evenly represented by AERONET stations in terms of amount and spatial distribution (see Fig. 2, 3<sup>rd</sup> column). The best coverage is found in Med-Sea and NorEur, in MidEas there are fewer stations but well distributed, whereas in NorAft the majority of the stations are located at the edges of the Sahara. The DOD seasonality is again identified over the dust emission and transport regions; however, huge biases between the two datasets like those obtained in SubSah during DJF ( $MB = -0.45$ ,  $RMSE = 0.62$ ) can be attributed to mesoscale processes like Haboobs (Roberts and Knippertz, 2012) that can affect ground-based measurements (i.e., AERONET), but remain undetected by the model or even by satellites due to coarser spatiotemporal resolution. Here we should note that over the dust-rich regions the regional AERONET DOD is significantly larger than the corresponding satellite-derived DOD because the method used to retrieve AERONET DOD excludes cases of mixed aerosol type (see Sect. 2.5), which increases the contribution of pure dust events to the sample, and this eventually increases the mean AERONET DOD.

#### 4.1.2 MONARCH coarse DOD compared to MIDAS, AEROIASI and AERONET

Repeating the same process, the MONARCH coarse DOD is compared against MIDAS, AEROIASI, and AERONET (Fig. 5). As the coarse DOD is a fraction of the total DOD, the annual mean coarse DOD of MONARCH, MIDAS, and AERONET shows the same spatial distribution as total DOD (Fig. 4). The temporal correlation between the MONARCH reanalysis and MIDAS, AEROIASI and AERONET (Fig. 5p-r) is generally higher near source and transport areas ( $CC$  up to 0.8), and diminishes towards the northern latitudes (i.e., north of  $40^\circ$  N). In fact, the comparison with AEROIASI even shows a negative correlation at these latitudes ( $CC < 0$ , Fig. 5q).  $RMSE$  (Fig. 5j-l) and  $FGE$  (Fig. 5m-o) spatial distribution is similar among MIDAS, AEROIASI and AERONET showing maximum  $RMSE (> 0.32)$  and minimum  $FGE (< 0.4)$  in the regions with the

strongest dust activity where the maximum absolute MB was also found (e.g., Bodélé Depression; Fig. 5g–i). In long-range transport regions, AEROIASI presents larger errors ( $RMSE > 0.08$  and  $MB < -0.07$ ) than MIDAS and AERONET.

The MONARCH reanalysis overestimates the coarse DOD over all the dust sources when compared to MIDAS and AEROIASI (Fig. 5g–h) with values that exceed 0.1 over the Bodélé Depression and its downwind areas as well as over the major dust sources of the western Sahara Desert. Again here, as in the case of DOD MB, a discontinuity in the MB for MIDAS is noted between land and oceans. The comparison against AERONET shows overall underestimations ( $MB < 0$ ) with maxima ( $MB < -0.1$ ) at stations situated downwind of the Bodélé Depression towards the Gulf of Guinea, in Cape Verde and close to the Registan Desert (Fig. 5i). The overestimations of MONARCH in the comparison with MIDAS over desert dust sources (Fig. 5g) are related to the fact that the size distribution of MIDAS is skewed toward finer sizes (see Sect. 3). Moreover, slight underestimations in Europe in the comparison against AERONET (Fig. 5i) can be attributed to the discrimination method applied (see Sect. 2.5) that can also allow large sea-salt particles or other coarse aerosol of local origin. The MONARCH reanalysis is in very good agreement with MIDAS over the remote regions of the North Atlantic and continental Europe, where MB is almost zero, whereas the comparison with AEROIASI away from the dust sources produced a very strong underestimate ( $MB < -0.1$ ). Moreover, the MB in Fig. 5h changes abruptly when moving from desert to remote regions because the coarse DOD provided by AEROIASI is consistently larger than 0.09 over the entire domain, even in remote regions, whereas it does not exceed 0.36 over the dust sources (Fig. 5d5e), in agreement with the findings in Sect. 3, that AEROIASI tends to underestimate coarse DOD close to desert dust sources and to overestimate it far away from them (Fig. 3h).

Finally, the regional metrics of the MONARCH coarse DOD, compared to MIDAS, AEROIASI and AERONET, were computed at annual and seasonal scale and are presented in Fig. S5, Fig. S6 and Fig. S7, respectively. Naturally, regional coarse DOD follows the cycle of the total DOD over the sub-regions associated with dust emission (NorAfr, MidEas and WesAsi), as the seasonal means of MIDAS, AEROIASI and the collocated MONARCH data show (Fig. S5 and Fig. S6). The intra-annual variability of the coarse dust particles long-range transport is well represented by MIDAS and MONARCH seasonal coarse DOD over TroAtl, AraSea and MedSea (maxima in JJA, JJA and MAM, respectively). The two datasets are in good agreement too, providing very low seasonal and annual MB values in those sub-regions. On the other hand, AEROIASI does not exhibit any seasonality over the maritime and the remote regions located north of  $40^\circ$  N, with no season-on-season changes in coarse DOD, which remain consistently greater than 0.1 (NorAtl, NorEur and Russia), probably linked to lack of sensitivity. AEROIASI shows a weak performance for detecting low DOD values in seasons and in regions where minimal dust activity is expected, as already shown in Fig. 3h. As a consequence, large biases ( $MB < -0.08$  and  $RMSE > 0.09$ ) and no correlation ( $CC \sim 0$ ) are obtained by the comparison with MONARCH coarse DOD.

Regarding the MONARCH versus AERONET comparison at regional and seasonal scale (Fig. S7), the typical patterns in seasonality are also found here. ~~The seasonal MB and RMSE values over the dust emission and dust transport regions correspond to those obtained by the total DOD comparison. On the other hand, over the remote regions, MB is higher in absolute terms because AERONET tends to overestimate coarse DOD ( $> 0.03$ ) in northern latitudes ( $>$  At AERONET sites located close to the dust sources (NorAfr and MidEas) and in their outflow regions (TroAtl and AraSea), the MONARCH reanalysis correctly provides maximum coarse DOD values in MAM and JJA. Moreover, the MONARCH reanalysis succeeds~~



in identifying the dry season months at the sites south of the Sahel (i.e., DJF and MAM in SubSah). However, MONARCH's annual and seasonal coarse DOD is almost everywhere lower than the values provided by AERONET ( $MB < 0$ ). This is due to the fact that the AERONET coarse DOD product can be contaminated by other coarse particles as well. The contribution of other aerosols can be insignificant in southern latitudes ( $< 40^\circ N$ ), providing greater seasonal and annual values than for where mineral dust is the dominant type, but under low dust conditions their impact increases. In fact, in the remote regions of NorAtl, NorEur and Russia, and in MedSea where sea-salt predominates in coastal stations, AERONET coarse DOD (Fig. S7) results in most seasons greater than AERONET total DOD (Fig. S3), which is impossible. AERONET's coarse DOD overestimates naturally lead to large relative biases compared to MONARCH coarse DOD ( $FGE > 1.17$ ), and thereby the validity of the MONARCH reanalysis evaluation results reported in those regions diminishes. On the other hand, in the regions where coarse DOD is higher, the seasonal results of both normalized metrics are very good ( $FGE < 1$  and  $CC > 0.7$ ) and quite stable. This means that the MONARCH reanalysis reproduces the seasonal variability of coarse DOD very well compared to AERONET, although not in absolute values. In fact, there are many similarities between the seasonal change of MONARCH and AERONET Coarse Mode Fraction (CMF), which is defined as the coarse DOD to total DOD ratio. For example, considering the seasonal DOD and coarse DOD in NorAfr (Figs. S3 and S7) the seasonality of MONARCH CMF (DJF: 26 %; MAM: 35 %; JJA: 70 %; SON: 49 %) is consistent with AERONET's (DJF: 21 %; MAM: 40 %; JJA: 68 %; SON: 44 %). This implies that the MONARCH reanalysis reproduces very efficiently the size distribution of the dust particles at the sites in the vicinity of the Sahara Desert.

## 4.2 Assessment through multi-sensor aggregation

### 4.2.1 MONARCH DOD compared to MIDAS+MISR product

Overall, the DOD comparison results against the three independent datasets (i.e., MIDAS, MISR and AERONET) shows that over the areas of most interest, with high dust activity throughout the year and greater number of measurements, the evaluation scores are consistent, despite the different features of each dataset, namely the raw data, the dust separation assumptions, the uncertainties and the spatiotemporal resolution and coverage. Consequently, the validity of the evaluation results is enhanced, leading to safer conclusions about the performance of the ~~model-~~MONARCH reanalysis.

Nevertheless, differences between the results obtained from the different datasets do exist in some cases. In particular, the results obtained by MIDAS and MISR over the North Atlantic differ in MB, RMSE and CC, and the same applies to CC between MIDAS and AERONET. These discrepancies may be due to several possible reasons related to the features of the datasets and the region. The uncertainties involved in the derivation of MIDAS, MISR and AERONET dust products inevitably contribute to their differences too. All satellite-based instruments have increased difficulty retrieving particle properties at low AOD - let alone the DOD fraction in regions where it is even lower - especially over some surface types for which the reflectance can negatively impact the retrieval quality. AERONET's discrimination method can also allow large sea-salt particles to be misclassified as dust, especially at coastal sites. Moreover, MISR has much less frequent sampling compared to MIDAS, whereas AERONET's fine temporal resolution permits the detection of sub-daily micro- and mesoscale dust activity

caused by local sources, that satellites' less frequent sampling can miss. Lastly, unfavorable observing conditions, such as cloud cover common at high latitudes especially during wintertime, in addition to basic sampling frequency, can also decrease the quality of DOD retrievals, for example due to unmasked cirrus clouds misclassified as dust.

As ~~However, as~~ shown in Fig. 4, in most regions that are subject to high DOD levels and frequent dust intrusions, the assessment results are not affected by the features of each dataset; instead, datasets from different sensors can be used in a complementary way to provide more solid insight into the performance of the MONARCH reanalysis. In particular, the regional results obtained from MIDAS (Fig. S1) and MISR (Fig. S2) were averaged to a final weighted mean (MIDAS+MISR), considering as weight the corresponding number N as it is described in Sect. 2.6, using the equations shown in Table A2. As mentioned earlier, the two datasets not only do not overlap but complement each other in terms of space and time, favoring the combination of their results. In particular, MIDAS covers Aqua's overpass time (13:30 LT), both over land and sea whereas MISR considers Terra's overpass time (10:30 LT) over sea. Moreover, MISR and MIDAS have different spatial and temporal resolution. Consequently, the two MONARCH reanalysis samples obtained by collocation with the satellite datasets are complementary to each other. The combined regional results from MIDAS and MISR are presented by region and by temporal scale, in Fig. S4; furthermore, the annual scores are displayed in maps in Fig. 6, to better understand the geographical distribution of the results.

The MONARCH DOD (Fig. 6a) and the multi-sensor aggregation DOD (Fig. 6b) present similar patterns, with small discrepancies in DOD values over and around the dust sources. In most sub-regions MB (Fig. 6c) ranges between  $-0.02$  and  $0.02$ , which is quite low in most cases compared to DOD values. Minimum differences are found in Russia (MB  $\sim 0$ ) as well as in dust source and outflow regions like SubSah (MB =  $0.01$ ), MidEas (MB =  $-0.01$ ) and MedSea (MB  $\sim 0$ ). The largest positive difference is found in NorAfr (MB =  $0.04$ ) which contains the Sahara Desert and the highest annual regional DOD values are simulated or observed there (DOD =  $0.29$  and  $0.25$  respectively); whereas, the lowest negative MB ( $-0.04$ ) is found in TroAtl and in AraSea, which are subject to frequent dust transport from the Sahara Desert and the Arabian Peninsula, respectively.

The regional RMSE (Fig. 6d) shows that the greatest differences between MONARCH reanalysis and observations occur in regions with the strongest dust activity, with values higher than  $0.15$  in MidEas, NorAfr, TroAtl and SubSah, whereas the minimum RMSE ( $0.03$ ) occurred in the remote region of NorEur. Conversely, the regional FGE (Fig. 6e) is maximized ( $> 1.8$ ) over the remote regions of NorAtl, NorEur and Russia, whereas the lowest values (FGE  $< 0.5$ ) are found in MidEas and NorAfr. The regional CC (Fig. 6f) shows a clear north to south positive gradient with minimum value (CC =  $0.49$ ) over Russia and maximum values (CC  $> 0.8$ ) in NorAfr and SubSah.

Considering all the results obtained from the evaluation metrics at annual scale, as listed in Fig. S4 and visualized in Fig. 6, among sub-regions where high dust concentrations are often observed by satellites (MIDAS+MISR DOD  $> 0.07$ ) the best combined scores are found in MidEas (MB =  $-0.01$ , FGE =  $0.43$ ), NorAfr (FGE =  $0.43$ , CC =  $0.84$ ) and MedSea (MB =  $0$ , RMSE =  $0.09$ ), demonstrating very good reanalysis the MONARCH reanalysis very good performance in reproducing the DOD levels and its spatiotemporal variability over the major dust source regions of MidEas and NorAfr as well as in the nearby outflow region of MedSea. Considering that in NorAfr and MidEas the two highest mean annual DOD values were recorded (MIDAS+MISR DOD =  $0.25$  and  $0.24$ , respectively), the lowest FGE implies that the biases with respect to the

MONARCH reanalysis are insignificant there. Moreover, the highest CC (0.84) in NorAfr indicates the model's reanalysis'  
690 correct simulation of the time evolution of dust emissions from the Sahara Desert. Similarly, in MedSea MONARCH MB  
reaches the perfect score, with quite low deviations from it according to RMSE, implying a very good performance of the  
MONARCH reanalysis under low DOD conditions (MIDAS+MISR DOD = 0.07) and sporadic dust intrusions throughout  
the year. Furthermore, the fact that those three sub-regions have the two top largest (NorAfr and MidEas) and the fourth  
largest (MedSea) N (Fig. 6g), shows the consistency of the MONARCH reanalysis when evaluated against a large number of  
695 observations and corroborates the evaluation results.

On the other hand, the combination of the regional annual scores reveals weak agreement between MONARCH reanalysis  
and observations over TroAtl (MB = -0.04, RMSE = 0.16) and WesAsi (MB = -0.02, CC = 0.66). The inter-comparison  
of the MIDAS+MISR and MONARCH DOD against AERONET observations (Fig. 2, 3<sup>rd</sup> column and Fig. 4 3<sup>rd</sup> column,  
respectively) shows that MIDAS+MISR DOD is in better agreement with AERONET compared to the MONARCH reanalysis,  
700 providing better scores in most of the common sites included in those two regions. In particular, the MONARCH reanalysis  
underestimates AERONET DOD by at least 0.1 (MB < -0.01) at the majority of the stations located in TroAtl and WesAsi,  
where MIDAS+MISR biases are usually lower than 0.07 (MB > -0.07). As far as TroAtl is concerned, this indicates that the  
MONARCH reanalysis simulates higher dust deposition rates underestimating the real amount of dust particles that travels  
towards the Atlantic Ocean; however, it captures very well the DOD spatiotemporal variability, as reflected by the strong  
705 correlation (CC = 0.8) found in this region (Fig. S4).

Lastly, the ability of the MONARCH reanalysis to correctly simulate the annual cycle of the regional dust activity was  
examined by computing the seasonally weighted means of the evaluation metrics for winter (DJF), spring (MAM), summer  
(JJA) and autumn (SON) (Fig. S4). In general, atmospheric dust emissions and transport are subject to seasonal variation,  
following the changes in wind conditions at synoptic scale; consequently, each sub-region presents a distinct seasonality. At  
710 first glance it can be seen that the color patterns of simulated and observed DOD are very similar, showing that the MONARCH  
reanalysis captures very well the annual dust cycle over all sub-regions. Particularly in regions where the presence of dust is  
predominant, the MONARCH reanalysis reproduces the DOD peaks in MAM and JJA; correspondingly, the minimum seasonal  
DOD values are correctly simulated in DJF and SON. Accordingly, the MB and RMSE seasonal patterns are directly related  
to the seasonal DOD variation, with maximum values in MAM and in JJA which weaken during SON or DJF, for all the  
715 sub-regions of interest. On the contrary, in northern sub-regions, patterns in seasonality are less pronounced because of the low  
presence of dust. The sign of the seasonal MB agrees with the sign of the annual MB, with the exception of SubSah, where  
low underestimations during JJA (MB = -0.02) are likely associated with mesoscale convective dust storms (e.g., Haboobs)  
that the model cannot simulate.

The MONARCH reanalysis performance in reproducing the regional dust cycle can be also assessed by the normalized  
720 parameters of FGE and CC which are less magnitude-dependent and are expected to remain invariable throughout the year. In  
fact, low FGE seasonal values exhibit remarkable intra-annual stability over the major dust emission regions of NorAfr ( $0.39 \leq$   
FGE  $\leq 0.49$ ) and MidEas ( $0.41 \leq$  FGE  $\leq 0.47$ ), where intense dust activity and strong seasonal variability have been recorded.  
In addition, over the main dust transport region of TroAtl, the seasonal fluctuation of the FGE is insignificant. Likewise, almost

all the sub-regions of interest present high CC values and weak seasonality, namely NorAfr ( $0.81 \leq CC \leq 0.85$ ), MidEas ( $0.72 \leq CC \leq 0.81$ ), TroAtl ( $0.76 \leq CC \leq 0.82$ ), AraSea ( $0.72 \leq CC \leq 0.77$ ) and MedSea ( $0.74 \leq CC \leq 0.76$ ). The minimum seasonal CC (0.38) found over Russia in DJF, along with all the scores for the same season computed in Russia and in NorEur, should be considered unreliable because the number of dust retrievals decreases significantly in the north of Europe during the DJF season ( $N \sim 0 \times 10^7$  in Russia and  $N = 0.15 \times 10^7$  in NorEur), as MIDAS covers only snow-free surfaces.

#### 4.2.2 MONARCH coarse DOD compared to MIDAS+IASI product

Following the same methodology, the coarse DOD comparison results from MIDAS (Fig. S5) and AEROIASI (Fig. S6) were combined on a regional scale. Again here the satellite datasets complement each other since the MODIS equatorial overpass time is 13:30 LT while IASI crosses the equator twice a day at 09:30 and 21:30 LT. The MIDAS+IASI scores are presented by region in Fig. S8 from which the annual means are illustrated in Fig. 7.

Deviations in coarse DOD between MONARCH reanalysis (Fig. 7a) and MIDAS+IASI (Fig. 7b) are evident in SubSah (MB = 0.04; Fig. 7c), and mainly in NorAfr where the maximum overestimation is observed (MB = 0.06), which is 50 % greater compared to the DOD MB over the same sub-region (Fig. 6c). This is a significant overestimation if we consider that the coarse DOD is a fraction of the total DOD. On the other hand, quasi-zero MB's were recorded in WesAsi, Russia and MedSea. Accordingly, the RMSE (Fig. 7d) exceeds 0.12 in NorAfr, SubSah and MidEas, whereas the best scores ( $RMSE \leq 0.04$ ) are recorded in NorAtl, NorEur and Russia. In contrast, the lowest FGE values ( $\leq 0.5$ ) can be found in MidEas and NorAfr and the highest ( $FGE \geq 1.9$ ) over the remote regions of NorAtl, NorEur and Russia (Fig. 7e). Lastly, the CC (Fig. 7f) exceeds 0.8 in NorAfr and SubSah, while over Russia a very low correlation is observed ( $CC = 0.37$ ), as the negative CC values recorded there during the MONARCH reanalysis versus AEROIASI comparison (Fig. 5q), affect the corresponding regional values (Fig. S6).

Considering all the regional annual results (Fig. S8), among sub-regions where high dust concentrations are often observed by satellites (MIDAS+IASI coarse DOD  $> 0.05$ ), the best scores are found in AraSea ( $FGE = 0.74$ ,  $CC = 0.78$ ), MedSea (MB = 0.01,  $RMSE = 0.07$ ) and TroAtl (MB =  $-0.01$ ,  $CC = 0.79$ ), which contain the main dust outflow pathways with moderate and sporadic coarse dust activity throughout the year. On the other hand, the MONARCH reanalysis seems to perform less efficiently over the African continent, namely in NorAfr (MB = 0.06,  $RMSE = 0.14$ ) and in SubSah (MB = 0.04,  $RMSE = 0.14$ ), where MONARCH seems to generate a surplus of coarse dust particles. Given that both sub-regions present the highest CC (0.83), the coarse dust emissions from the Sahara Desert seem to be overestimated by a constant factor during the entire study period.

Focusing in those two regions, the inter-comparison of the MIDAS+IASI and MONARCH coarse DOD against AERONET (Fig. 3, 3<sup>rd</sup> column and Fig. 5 3<sup>rd</sup> column, respectively) shows that MONARCH coarse DOD is in better agreement with AERONET compared to MIDAS+IASI, providing better scores in most of the common sites. Especially at common sites located in the Sahara Desert, MONARCH MB is limited between  $-0.04$  and  $-0.01$  showing very small differences with AERONET (Fig. 5i, see NorAfr) considering that AERONET coarse DOD at these sites exceeds 0.14 (Fig. 5f, NorAfr); whereas MIDAS+IASI MB varies from  $-0.1$  to 0.1, implying significant deviations from the ground-based measurements

(Fig. 3i, NorAfr). Actually, the MIDAS+IASI product at those sites is mostly biased due to AEROIASI's strong over- and underestimations (Fig. 3h, NorAfr), whereas MIDAS reproduces quite well AERONET coarse DOD ( $-0.04 < MB < 0$ ; Fig. 3g, NorAfr). On the other hand, the MONARCH [reanalysis](#) annual regional scores commented in the previous paragraph are dominated by MIDAS contribution (see annual values of Fig. S5 and Fig. S8), due to a larger number of MODIS observations. Considering that MIDAS coarse DOD is derived using  $0.5 \mu\text{m}$  as a cut-off radius whereas MONARCH uses  $0.6 \mu\text{m}$ , it means that in case of common radius value, the MONARCH versus MIDAS MB results over NorAfr and SubSah would be even larger. This again should be attributed to MERRA-2 fine/coarse DOD ratio which eventually underestimates MIDAS coarse DOD, especially over areas of high dust activity (Fig. 3g). In conclusion, the discrepancies between MONARCH coarse DOD and both satellite datasets over the African continent are most likely due to underestimations in MIDAS and AEROIASI coarse DOD retrievals.

Any seasonality in the performance of the [MONARCH reanalysis](#) in reproducing the coarse DOD can be assessed by the seasonal values of the metrics computed at regional scale (Fig. S8). The reanalysis simulates very well the annual cycle of coarse dust at both emission and transport regions where coarse DOD seasonality is intense and peak activity occurs in MAM or in JJA, depending on the sub-region, exactly as was observed by the two satellite instruments. The discrepancies are more pronounced and subject to seasonal variation over the main dust source regions of NorAfr and MidEas, where MB is maximized during JJA, when coarse dust loads are higher, and weakens during SON. A reverse pattern is recorded in SubSah, TroAtl and MedSea where the seasonal minima ( $MB \sim 0$ ) corresponds to seasons of quite high coarse DOD values (i.e., JJA, DJF and MAM, respectively). Moreover, in MedSea and mostly in WesAsi seasonal MB remains remarkably low and stable throughout the year, despite the seasonal coarse DOD fluctuations. On the other hand, RMSE seasonal pattern follows consistently the corresponding coarse DOD annual cycle of each sub-region.

Regarding the normalized parameters FGE and CC, both dust emission and transport sub-regions present values with significant stability throughout the year. This actually reveals a small degree of dependence between [MONARCH reanalysis](#) performance and coarse DOD seasonality. In particular, the lowest FGE seasonality can be found in regions with strong seasonal changes in coarse DOD, namely in NorAfr ( $0.45 \leq FGE \leq 0.56$ ) and MidEas ( $0.43 \leq FGE \leq 0.51$ ). Similarly, seasonal CC values exhibit intra-annual stability in most of the source and transport regions, such as NorAfr ( $0.79 \leq CC \leq 0.84$ ), MidEas ( $0.72 \leq CC \leq 0.80$ ), TroAtl ( $0.74 \leq CC \leq 0.82$ ), AraSea ( $0.71 \leq CC \leq 0.76$ ) and MedSea ( $0.72 \leq CC \leq 0.74$ ). On the other hand, in northern regions where the number of MIDAS observations is lower compared to southern regions, and AEROIASI's contribution to the combined product increases, the seasonal CC values decrease and significant seasonality is noted. This should not be attributed to any [MONARCH reanalysis](#) uncertainties but to the low quality of AEROIASI retrievals in northern latitudes, as it was concluded in Sect. 3 (Fig. 3), which can bias the regional results of the comparison.

Overall, the seasonal scores of MONARCH total and coarse DOD derived from the comparison with MIDAS+MISR (Fig. S4) and MIDAS+IASI (Fig. S8) respectively, exhibit a similar degree of seasonality by region and by statistical parameter. In regions most affected by dust the results are comparable, with best agreements on CC seasonal scores, implying that the performance of the [MONARCH reanalysis](#) for both total and coarse DOD is consistent.

## 5 Conclusions

MONARCH dust reanalysis is an advanced dust decadal (2007–2016) regional reanalysis, based on the weather–aerosol–chemistry MONARCH model, providing a continuous 3D representation of atmospheric desert dust over the NAMEE region, with high spatial and temporal resolution. Providing thorough information on dust variations and trends, this product can be exploited for the development of climate services tailored to key socio–economic sectors, focusing on those that can be significantly affected by atmospheric dust, such as health, transportation and solar energy industry. Therefore, the assessment of the [MONARCH](#) reanalysis performance is of great importance in order to identify its strengths and potential weaknesses, and to be considered in future applications.

Here [in particular](#), we seek to assess the performance of the [MONARCH](#) reanalysis in reproducing the total [column variables of total](#) and coarse DOD using dust products derived from MODIS, MISR and IASI space-borne instruments along with ground-based remote-sensing measurements from AERONET. Instead of using a single dataset as reference, in the present analysis different observational-based products were combined, which together provide better coverage of ~~the model~~ [MONARCH](#)'s spatiotemporal domain. However, each satellite sensor has its own strengths, limitations, and uncertainties. The total and coarse DOD products of the reference datasets (i.e., MIDAS, MISR, and AEROIASI) were obtained following different retrieval techniques and assumptions; limitations on each dust characterization technique introduce uncertainties into the DOD products. Therefore, an additional advantage of using different observational reference datasets is the ability to perform cross-validation of the ~~model's~~ [MONARCH reanalysis](#) performance, based on the results obtained from each dataset. By collating the comparison results obtained from the different datasets we can identify biases caused by retrieval uncertainties and assess their contribution to the evaluation results.

Moreover, prior to the [MONARCH](#) reanalysis assessment, we checked the quality of the satellite-based dust products by applying collocated inter-comparison among the different datasets, using AERONET observations as the reference dataset. Significant discrepancies between satellite and ground-based products over certain regions should be considered as a potential source of skewness for the subsequent ~~model~~ [reanalysis](#) assessment. More specifically, MIDAS and MISR tend to underestimate total DOD in areas close to the dust sources and slightly overestimate it in remote regions, whereas MIDAS underestimates coarse DOD everywhere; however, both MIDAS and MISR exhibit high correlation ( $CC > 0.8$ ) and low relative bias ( $FGE < 0.4$ ) at most sites where high dust concentrations are recorded (latitudes  $< 40^\circ$  N). Lastly, AEROIASI shows moderate correlations ( $0.4 < CC < 0.8$ ) for stations south of  $40^\circ$  N, but overestimates coarse DOD ( $MB > 0.07$ ) in remote regions (latitudes  $> 40^\circ$  N), showing a weakness in capturing the temporal variations of coarse DOD in these areas at annual or seasonal scales, as indicated by the low correlation with AERONET.

Taking into account these outcomes, the MONARCH reanalysis assessment was based on the comparison against AERONET and the satellite products, highlighting the similarities among the obtained results for drawing safer conclusions. According to our findings, the MONARCH reanalysis reproduces very well the spatial distribution of atmospheric dust across the NAMEE region, identifying the major dust emission hotspots located in the Sahara Desert and the Middle East, and the main dust transport pathways toward the adjacent maritime regions of the Atlantic Ocean, the Arabian Sea and the Mediterranean Sea.



Moreover, the [MONARCH](#) reanalysis is able to reproduce very well the total and coarse DOD seasonal variability with good accuracy, especially over the aforementioned areas (annual and seasonal CC values consistently greater than 0.6 and up to 0.87), indicating that the reanalysis captures quite well the annual dust cycle both over the sources and the nearby outflow regions.

830 Quantitatively, according to the evaluation scores, the MONARCH reanalysis seems to simulate more emitted and less transported dust particles. [This could be due to several factors such as having observational constraint mostly over land only or potential issues in the dust deposition and transport in the underlying model.](#) The comparison with the satellite multi-sensor products at regional scale shows that on average, the [MONARCH](#) reanalysis produces slightly higher DOD values over Africa and lower DOD over the Atlantic Ocean and the Arabian Sea. More specifically, the maximum annual overestimation  
835 in total DOD was found in NorAfr (MB = 0.04), the sub-region which contains the Sahara Desert, which is rather insignificant compared to the mean DOD value obtained there from the satellite sensors (MIDAS+MISR DOD = 0.25). Similarly, the MONARCH reanalysis simulates higher coarse DOD over the Sahara Desert compared to the multi-sensor product (MIDAS+IASI); however, the accuracy of this outcome remains questionable due to MIDAS systematic underestimations of the coarse DOD product. On the other hand, the minimum negative MB was recorded over the maritime regions of TroAtl and  
840 AraSea, both for total DOD (MB = -0.04) and coarse DOD (MB = -0.02), indicating a slight underestimation in simulating the exact transported dust quantity in the main downstream directions during the study period. Finally, as an exception to that general conclusion, a near-zero DOD MB was recorded over the MedSea and a near-zero coarse DOD MB over WesAsi, which are considered as dust transport and dust source region, respectively.

The calculation of the FGE, which corresponds to the absolute relative bias of the [modelreanalysis](#), and the CC, which  
845 represents the spatiotemporal correlation between the simulations and the multi-sensor products, shows that the [MONARCH](#) reanalysis performs better (low FGE and high CC) over dust sources and over areas frequently affected by dust transport, whereas the reanalysis scores diminish towards the remote regions located in the northern parts of the study region, where very low annual DOD values are recorded. Both statistical parameters are normalized, allowing comparisons between the total DOD and coarse DOD assessment results. In fact, the annual FGE calculated for each sub-region presents small differences  
850 between total and coarse DOD, whereas the CC is almost identical, especially in regions of high dust concentrations, indicating that the regional scores depend more on the region and its dust levels than on the evaluated variable. According to our regional results, the sub-regions of NorAfr, MidEas, AraSea and TroAtl provide FGE lower than 1 and CC higher than 0.78 for both variables. These good results are corroborated by the high number of available observations used for the [MONARCH](#) reanalysis assessment in these sub-regions. On the other hand, the remote sub-regions of NorEur and Russia are characterized by very  
855 large errors (FGE > 1.93) and low correlation (CC < 0.6). In this case, the very low availability of MIDAS observations and the significant overestimations of AEROIASI products over these regions prevents us from drawing strong conclusions. To sum up, the MONARCH reanalysis is very reliable over all the regions of frequent dust activity and high dust concentrations where the best normalized statistics (low FGE and high CC) are presented and coincide with large N values, indicating the consistency of the [MONARCH](#) reanalysis when compared against a large number of observations and consequently its very  
860 good performance.

**Table A1.** Summary of the statistical metrics that were used in the model [reanalysis](#) evaluation.

| Statistic parameter     | Equation  | Range                  | Perfect score |
|-------------------------|---|------------------------|---------------|
| Mean Bias               | $MB_d = \bar{M}_d - \bar{O}_d$  | $-\infty$ to $+\infty$ | 0             |
| Root Mean Square Error  | $RMSE_d = \sqrt{\frac{1}{N_d} \cdot \sum_{i=1}^N (M_i - O_i)^2}$  | 0 to $+\infty$         | 0             |
| Fractional Gross Error  | $FGE_d = \frac{2}{N_d} \cdot \sum_{i=1}^N \left  \frac{M_i - O_i}{M_i + O_i} \right $   | 0 to 2                 | 0             |
| Correlation Coefficient | $CC_d = \frac{\sum_{i=1}^N (M_i - \bar{M}_d) \cdot (O_i - \bar{O}_d)}{\sqrt{\sum_{i=1}^N (M_i - \bar{M}_d)^2} \cdot \sqrt{\sum_{i=1}^N (O_i - \bar{O}_d)^2}}$ | -1 to 1                | 1             |

The present work shows that using data from different sensors increases the observational coverage, allowing one to assess a larger sample of model data and get better representativeness. More importantly, through the synergy of satellite sensors that perform differently depending on weather conditions, surface type and atmospheric dust concentration, it is possible to better assess the performance of modeling products in conditions where the sensitivity of one sensor to dust particles is higher than another. In this direction, satellite missions like NASA's EMIT (Earth Surface Mineral Dust Source Investigation; <https://earth.jpl.nasa.gov/emit>, last access: ~~14-September-2022~~[30 March 2023](#)) instrument or ESA's EarthCARE (Earth Cloud, Aerosol and Radiation Explorer; <https://earth.esa.int/eogateway/missions/earthcare>, last access: ~~14-September-2022~~[30 March 2023](#)) satellite with active sensors on board, in conjunction with improving observational capabilities from the ground through regional research infrastructures, e.g., ACTRIS ([www.actris.eu](http://www.actris.eu), last access: ~~14-September-2022~~[30 March 2023](#)), and international initiatives such as GALION (WMO, 2007), could contribute to overcoming current limitations.

*Data availability.* The MONARCH reanalysis dataset (Di Tomaso et al., 2021) is available at <http://hdl.handle.net/21.12146/c6d4a608-5de3-47f6-a004-67cb1d498d98> (last access: 30 March 2023). The MIDAS dataset (Gkikas et al., 2020) is available at <https://doi.org/10.5281/zenodo.4244106>. AERONET Version 3 data are available from the AERONET web site (<https://aeronet.gsfc.nasa.gov>, last access: 30 March 2023). The MISR standard data products can be found at the NASA Langley Atmospheric Data Center (ASDC) Distributed Archive Center (DAAC) (<https://asdc.larc.nasa.gov>, last access: 30 March 2023). AEROIASI data can be provided upon request to the principal investigator of the satellite data: Juan Cuesta, LISA/UPEC, [cuesta@lisa.ipsl.fr](mailto:cuesta@lisa.ipsl.fr).

## Appendix A: Evaluation metrics

The evaluation metrics that were used to quantify the performance of the [model](#) reanalysis products ( $M_i$ ) versus the observational-based retrievals ( $O_i$ ) are presented in Table A1-, [where](#):

880 [where](#):-

$$\bar{M}_d = \frac{1}{N_d} \cdot \sum_{i=1}^N M_i \quad (A1)$$

$$\sigma M_d = \sqrt{\frac{1}{N_d} \cdot \sum_{i=1}^N (M_i - \bar{M}_d)^2} \quad (\text{A2})$$

$$\bar{O}_d = \frac{1}{N_d} \cdot \sum_{i=1}^N O_i \quad (\text{A3})$$

$$\sigma O_d = \sqrt{\frac{1}{N_d} \cdot \sum_{i=1}^N (O_i - \bar{O}_d)^2} \quad (\text{A4})$$

885 are the mean and the standard deviation of the reanalysis (Eq. A1–A2) and the observed DOD (Eq. A3–A4); N indicates the total number of collocated and concurrent  $M_i$ - $O_i$  pairs. The subscript d denotes the observational dataset used in the calculations.

MB captures the average deviation between the two datasets. Negative/positive MB indicates underestimation/overestimation of the reanalysis with respect to the observations. It theoretically ranges from  $-\infty$  to  $+\infty$  and its perfect score is 0.

890 RMSE represents the root mean square difference between the reanalysis and observations. It is a measure of how spread out these differences are. RMSE is strongly dominated by the largest differences due to the squaring operation. It ranges between 0 and  $+\infty$  and its perfect score is 0.

FGE is a measure of the mean absolute relative bias where the difference between reanalysis and observation is normalized by their mean value. It is a positively defined indicator that behaves symmetrically with respect to under- and overestimation, 895 without over emphasizing outliers. FGE ranges from 0 to 2 (i.e., from 0 to 200 %), where 0 indicates a perfect agreement and values close to 1 or greater indicate very poor agreement.

CC indicates the extent to which spatial and temporal patterns in the reanalysis match those in the observations, quantifying their correlation and dependence. It ranges between  $-1$  and  $1$ , where  $-1$  means perfect anti-correlation, 0 means no correlation, and 1 indicates perfect correlation.

900 The statistical results obtained by the comparison between the reanalysis and each reference satellite dataset can be aggregated in order to get total average scores by weighting the metrics of Table A1 by the number of observations  $N_d$  provided by each dataset, using the equations of Table A2, where:

where:-

$$\bar{M} = \frac{\sum_{d=1}^2 N_d \cdot \bar{M}_d}{\sum_{d=1}^2 N_d} \quad (\text{A5})$$

905 
$$\sigma M = \sqrt{\frac{\sum_{d=1}^2 N_d \cdot [\sigma M_d^2 + (\bar{M}_d - \bar{M})^2]}{\sum_{d=1}^2 N_d}} \quad (\text{A6})$$

**Table A2.** Weighted mean of the evaluation metrics obtained by different reference satellite datasets.

| Statistic parameter     | Equation   |
|-------------------------|--|
| Mean Bias               | $MB = \frac{\sum_{d=1}^2 N_d \cdot MB_d}{\sum_{d=1}^2 N_d}$  |
| Root Mean Square Error  | $RMSE = \sqrt{\frac{\sum_{d=1}^2 N_d \cdot RMSE_d^2}{\sum_{d=1}^2 N_d}}$   |
| Fractional Gross Error  | $FGE = \frac{\sum_{d=1}^2 N_d \cdot FGE_d}{\sum_{d=1}^2 N_d}$  |
| Correlation Coefficient | $CC = \frac{\sum_{d=1}^2 N_d \cdot [CC_d \cdot \sigma M_d \cdot \sigma O_d + (\bar{M}_d - \bar{M}) \cdot (\bar{O}_d - \bar{O})]}{\sqrt{\sum_{d=1}^2 N_d \cdot [\sigma M_d^2 + (\bar{M}_d - \bar{M})^2]} \cdot \sqrt{\sum_{d=1}^2 N_d \cdot [\sigma O_d^2 + (\bar{O}_d - \bar{O})^2]}}$ |

$$\bar{O} = \frac{\sum_{d=1}^2 N_d \cdot \bar{O}_d}{\sum_{d=1}^2 N_d} \quad (A7)$$

$$\sigma O = \sqrt{\frac{\sum_{d=1}^2 N_d \cdot [\sigma O_d^2 + (\bar{O}_d - \bar{O})^2]}{\sum_{d=1}^2 N_d}} \quad (A8)$$

are the weighted mean and the combined standard deviation of the reanalysis (Eq. A5–A6) and the aggregated satellite-based dust products (i.e., MIDAS+MISR for DOD and MIDAS+AEROIASI for coarse DOD) (Eq. A7–A8). The subscript d denotes the satellite dataset used in the calculations (d = 1 MIDAS and d = 2 MISR for DOD; as well as d = 1 MIDAS and d = 2 AEROIASI for coarse DOD).

*Author contributions.* MM, LM, SB and EDT designed the study and the whole analysis. SB collected and prepared the datasets. MM processed all the datasets and performed the data analysis. SC contributed to the statistical analysis of the data. MM wrote the initial manuscript with contributions from LM and ST. MM, LM, SB, EDT and CPGP discussed the main results. RK, SB, EDT, CPGP, AG, JC, ST, CD and OJ reviewed and edited the manuscript. RK contributed also to the part of the paper relating to MISR data. EDT contributed also to the part relating to the MONARCH reanalysis data. AG contributed also to the part relating to MIDAS data. JC and PF contributed also to the part relating to AEROIASI data. All co-authors contributed to the final editing of the manuscript. [MM, LM, EDT, SB, JC and AG responded to the comments of two anonymous reviewers and revised the manuscript.](#) LM supervised the entire work.

*Competing interests.* The authors declare that they have no conflict of interest.

*Acknowledgements.* The authors thank all the Principal Investigators and their staff for establishing and maintaining the NASA and PHOTONS AERONET sites, and the MODIS and MISR mission scientists and associated NASA personnel for the production of the data used in this study. [Likewise, two anonymous reviewers are acknowledged, who provided constructive comments and useful suggestions that](#)

[improved the quality of the present manuscript](#). BSC co-authors acknowledge PRACE (eDUST, eFRAGMENT1 and eFRAGMENT2) and RES (AECT-2019-3-0001, AECT-2020-1-0007, AECT-2020-3-0013) for awarding access to MareNostrum at the BSC and for providing  
925 technical support.

*Financial support.*

This research has been supported by the DustClim project which is part of ERA4CS, an ERA-NET programme initiated by JPI Climate with co-funding by the European Union's Horizon 2020 research and innovation programme (Grant no 690462). The authors acknowledge the ACTRIS-IMP (Implementation project), funded by the European Union's Horizon  
930 2020 research and innovation programme (Grant no 871115). Michail Mytilinaios, Sergio Ciamprone and Claudio Dema have received funding from CIR01\_00015 - PER-ACTRIS-IT "Potenziamento della componente italiana della Infrastruttura di Ricerca Aerosol, Clouds and Trace Gases Research Infrastructure-Rafforzamento del capitale umano" - Avviso MUR D.D. n. 2595 del 24.12.2019 Piano Stralcio "Ricerca e Innovazione 2015–2017". BSC co-authors acknowledge support from the European Research Council under the European Union's Horizon 2020 research and innovation programme (grant n. 773051;  
935 FRAGMENT), the AXA Research Fund (AXA Chair on Sand and Dust Storms), and the contribution agreement between AEMET and BSC to carry out development and improvement activities of the products and services supplied by the World Meteorological Organization (WMO) Barcelona Dust Regional Center (i.e., the WMO Sand and Dust Storm Warning Advisory and Assessment System (SDS-WAS) Regional Center for Northern Africa, the Middle East and Europe). The work of Ralph Kahn is support in part by the NASA Aerosol-Cloud Modeling and Analysis Program under Richard Eckman, and the NASA  
940 Earth Observing System Terra and MISR projects. Antonis Gkikas acknowledges support by the Hellenic Foundation for Research and Innovation (H.F.R.I.) under the "2<sup>nd</sup> Call for H.F.R.I. Research Projects to support Post-Doctoral Researchers" (Project Acronym: ATLANTAS, Project Number: 544). The MIDAS dataset has been developed in the framework of the DUST-GLASS project (grant no. 749461; European Union's Horizon 2020 Research and Innovation programme under the Marie Skłodowska-Curie Actions). The AEROIASI product is developed at the LISA laboratory with the financial support of  
945 the IASI-TOSCA (Terre, Océan, Surface Continentale et Atmosphère) project from the Centre National des Etudes Spatiales (CNES) and technical assistance of the AERIS French national data centre. IASI is a joint mission of EUMETSAT and CNES.

## References

- Abdou, W. A., Diner, D. J., Martonchik, J. V., Bruegge, C. J., Kahn, R. A., Gaitley, B. J., Crean, K. A., Remer, L. A., and Holben, B.: Comparison of coincident Multiangle Imaging Spectroradiometer and Moderate Resolution Imaging Spectroradiometer aerosol optical depths over  
950 land and ocean scenes containing Aerosol Robotic Network sites, *J. Geophys. Res.-Atmos.*, 110, <https://doi.org/10.1029/2004JD004693>, 2005.
- Al-Hemoud, A., Al-Sudairawi, M., Neelamanai, S., Naseeb, A., and Behbehani, W.: Socioeconomic effect of dust storms in Kuwait, *Arab. J. Geosci.*, 10, <https://doi.org/10.1007/s12517-016-2816-9>, 2017.
- Amiridis, V., Marinou, E., Tsekeri, A., Wandinger, U., Schwarz, A., Giannakaki, E., Mamouri, R., Kokkalis, P., Biniotoglou, I., Solomos,  
955 S., Herekakis, T., Kazadzis, S., Gerasopoulos, E., Proestakis, E., Kottas, M., Balis, D., Papayannis, A., Kontoes, C., Kourtidis, K., Pappagiannopoulos, N., Mona, L., Pappalardo, G., Le Rille, O., and Ansmann, A.: LIVAS: a 3-D multi-wavelength aerosol/cloud database based on CALIPSO and EARLINET, *Atmos. Chem. Phys.*, 15, 7127–7153, <https://doi.org/10.5194/acp-15-7127-2015>, 2015.
- Basart, S., Pérez, C., Cuevas, E., Baldasano, J. M., and Gobbi, G. P.: Aerosol characterization in Northern Africa, Northeastern Atlantic, Mediterranean Basin and Middle East from direct-sun AERONET observations, *Atmos. Chem. Phys.*, 9, 8265–8282,  
960 <https://doi.org/10.5194/acp-9-8265-2009>, 2009.
- Benedetti, A., Reid, J. S., Knippertz, P., Marsham, J. H., Di Giuseppe, F., Rémy, S., Basart, S., Boucher, O., Brooks, I. M., Menut, L., Mona, L., Laj, P., Pappalardo, G., Wiedensohler, A., Baklanov, A., Brooks, M., Colarco, P. R., Cuevas, E., da Silva, A., Escribano, J., Flemming, J., Huneus, N., Jorba, O., Kazadzis, S., Kinne, S., Popp, T., Quinn, P. K., Sekiyama, T. T., Tanaka, T., and Terradellas, E.: Status and future of numerical atmospheric aerosol prediction with a focus on data requirements, *Atmos. Chem. Phys.*, 18, 10 615–10 643,  
965 <https://doi.org/10.5194/acp-18-10615-2018>, 2018.
- Bristow, C. S., Hudson-Edwards, K. A., and Chappell, A.: Fertilizing the Amazon and equatorial Atlantic with West African dust, *Geophys. Res. Lett.*, 37, <https://doi.org/10.1029/2010GL043486>, 2010.
- Buchard, V., Randles, C. A., da Silva, A. M., Darmenov, A., Colarco, P. R., Govindaraju, R., Ferrare, R., Hair, J., Beyersdorf, A. J., Ziemba, L. D., and Yu, H.: The MERRA-2 aerosol reanalysis, 1980 onward. Part II: Evaluation and case studies, *J. Climate*, 30, 6851–6872,  
970 <https://doi.org/10.1175/JCLI-D-16-0613.1>, 2017.
- Cadelis, G., Tourres, R., and Molinie, J.: Short-Term Effects of the Particulate Pollutants Contained in Saharan Dust on the Visits of Children to the Emergency Department due to Asthmatic Conditions in Guadeloupe (French Archipelago of the Caribbean), *PLOS ONE*, 9, 1–11, <https://doi.org/10.1371/journal.pone.0091136>, 2014.
- Carslaw, K. S., Boucher, O., Spracklen, D. V., Mann, G. W., Rae, J. G. L., Woodward, S., and Kulmala, M.: A review of natural aerosol interactions and feedbacks within the Earth system, *Atmos. Chem. Phys.*, 10, 1701–1737, <https://doi.org/10.5194/acp-10-1701-2010>,  
975 2010.
- Clarisse, L., Clerbaux, C., Franco, B., Hadji-Lazaro, J., Whitburn, S., Kopp, A. K., Hurtmans, D., and Coheur, P.-F.: A decadal data set of global atmospheric dust retrieved from IASI satellite measurements, *J. Geophys. Res.-Atmos.*, 124, 1618–1647, <https://doi.org/10.1029/2018JD029701>, 2019.
- 980 Costa, S. C., Diniz, A. S. A., and Kazmerski, L. L.: Dust and soiling issues and impacts relating to solar energy systems: Literature review update for 2012–2015, *Renewable and Sustainable Energy Reviews*, 63, 33–61, <https://doi.org/10.1016/j.rser.2016.04.059>, 2016.



- Cuesta, J., Eremenko, M., Flamant, C., Dufour, G., Laurent, B., Bergametti, G., Höpfner, M., Orphal, J., and Zhou, D.: Three-dimensional distribution of a major desert dust outbreak over East Asia in March 2008 derived from IASI satellite observations, *J. Geophys. Res.-Atmos.*, 120, 7099–7127, <https://doi.org/10.1002/2014JD022406>, 2015.
- 985 Cuesta, J., Flamant, C., Gaetani, M., Knippertz, P., Fink, A. H., Chazette, P., Eremenko, M., Dufour, G., Di Biagio, C., and Formenti, P.: Three-dimensional pathways of dust over the Sahara during summer 2011 as revealed by new Infrared Atmospheric Sounding Interferometer observations, *Q. J. Roy. Meteor. Soc.*, 146, 2731–2755, <https://doi.org/10.1002/qj.3814>, 2020.
- Cuevas, E., Camino, C., Benedetti, A., Basart, S., Terradellas, E., Baldasano, J. M., Morcrette, J. J., Marticorena, B., Goloub, P., Mortier, A., Berjón, A., Hernández, Y., Gil-Ojeda, M., and Schulz, M.: The MACC-II 2007–2008 reanalysis: atmospheric dust evaluation and  
990 characterization over northern Africa and the Middle East, *Atmos. Chem. Phys.*, 15, 3991–4024, <https://doi.org/10.5194/acp-15-3991-2015>, 2015.
- Di Tomaso, E., Schutgens, N. A. J., Jorba, O., and Pérez García-Pando, C.: Assimilation of MODIS Dark Target and Deep Blue observations in the dust aerosol component of NMMB-MONARCH version 1.0, *Geosci. Model Dev.*, 10, 1107–1129, <https://doi.org/10.5194/gmd-10-1107-2017>, 2017.
- 995 Di Tomaso, E., Escribano, J., Basart, S., Macchia, F., Benincasa, F., Bretonnière, P.-A., Buñuel, A., Castrillo, M., Gonçalves, M., Jorba, O., Klose, M., Montané Pinto, G., Olid, M., and Pérez García-Pando, C.: MONARCH high-resolution reanalysis data set of desert dust aerosol over Northern Africa, the Middle East and Europe, BSC, THREDDS, <http://hdl.handle.net/21.12146/c6d4a608-5de3-47f6-a004-67cb1d498d98>, last access: 30 March 2023, 2021.
- Di Tomaso, E., Escribano, J., Basart, S., Ginoux, P., Macchia, F., Barnaba, F., Benincasa, F., Bretonnière, P.-A., Buñuel, A., Castrillo,  
1000 M., Cuevas, E., Formenti, P., Gonçalves, M., Jorba, O., Klose, M., Mona, L., Montané Pinto, G., Mytilinaios, M., Obiso, V., Olid, M., Schutgens, N., Votsis, A., Werner, E., and Pérez García-Pando, C.: The MONARCH high-resolution reanalysis of desert dust aerosol over Northern Africa, the Middle East and Europe (2007–2016), *Earth Syst. Sci. Data*, 14, 2785–2816, <https://doi.org/10.5194/essd-14-2785-2022>, 2022.
- Diner, D., Beckert, J., Reilly, T., Bruegge, C., Conel, J., Kahn, R., Martonchik, J., Ackerman, T., Davies, R., Gerstl, S., Gordon, H., Muller,  
1005 J.-P., Myneni, R., Sellers, P., Pinty, B., and Verstraete, M.: Multi-angle Imaging SpectroRadiometer (MISR) instrument description and experiment overview, *IEEE T. Geosci. Remote*, 36, 1072–1087, <https://doi.org/10.1109/36.700992>, 1998.
- Dubovik, O., Holben, B., Eck, T. F., Smirnov, A., Kaufman, Y. J., King, M. D., Tanré, D., and Slutsker, I.: Variability of absorption and optical properties of key aerosol types observed in worldwide locations, *J. Atmos. Sci.*, 59, 590–608, [https://doi.org/10.1175/1520-0469\(2002\)059<0590:VOAAOP>2.0.CO;2](https://doi.org/10.1175/1520-0469(2002)059<0590:VOAAOP>2.0.CO;2), 2002.
- 1010 Eck, T. F., Holben, B. N., Reid, J. S., Dubovik, O., Smirnov, A., O’Neill, N. T., Slutsker, I., and Kinne, S.: Wavelength dependence of the optical depth of biomass burning, urban, and desert dust aerosols, *J. Geophys. Res.-Atmos.*, 104, 31333–31349, <https://doi.org/10.1029/1999JD900923>, 1999.
- Escribano, J., Di Tomaso, E., Jorba, O., Klose, M., Gonçalves Ageitos, M., Macchia, F., Amiridis, V., Baars, H., Marinou, E., Proestakis, E., Urbanneck, C., Althausen, D., Bühl, J., Mamouri, R.-E., and Pérez García-Pando, C.: Assimilating spaceborne lidar dust extinction can  
1015 improve dust forecasts, *Atmos. Chem. Phys.*, 22, 535–560, <https://doi.org/10.5194/acp-22-535-2022>, 2022.
- Flaounas, E., Kotroni, V., Lagouvardos, K., Kazadzis, S., Gkikas, A., and Hatzianastassiou, N.: Cyclone contribution to dust transport over the Mediterranean region, *Atmos. Sci. Lett.*, 16, 473–478, <https://doi.org/10.1002/asl.584>, 2015.
- Gelaro, R., McCarty, W., Suárez, M. J., Todling, R., Molod, A., Takacs, L., Randles, C. A., Darmenov, A., Bosilovich, M. G., Reichle, R., Wargan, K., Coy, L., Cullather, R., Draper, C., Akella, S., Buchard, V., Conaty, A., da Silva, A. M., Gu, W., Kim, G.-K., Koster, R.,

- 1020 Lucchesi, R., Merkova, D., Nielsen, J. E., Partyka, G., Pawson, S., Putman, W., Rienecker, M., Schubert, S. D., Sienkiewicz, M., and Zhao, B.: The Modern-Era Retrospective Analysis for Research and Applications, Version 2 (MERRA-2), *J. Climate*, 30, 5419–5454, <https://doi.org/10.1175/JCLI-D-16-0758.1>, 2017.
- Giles, D. M., Holben, B. N., Eck, T. F., Sinyuk, A., Smirnov, A., Slutsker, I., Dickerson, R. R., Thompson, A. M., and Schafer, J. S.: An analysis of AERONET aerosol absorption properties and classifications representative of aerosol source regions, *J. Geophys. Res.-Atmos.*, 1025 117, <https://doi.org/10.1029/2012JD018127>, 2012.
- Giles, D. M., Sinyuk, A., Sorokin, M. G., Schafer, J. S., Smirnov, A., Slutsker, I., Eck, T. F., Holben, B. N., Lewis, J. R., Campbell, J. R., Welton, E. J., Korkin, S. V., and Lyapustin, A. I.: Advancements in the Aerosol Robotic Network (AERONET) Version 3 database – automated near-real-time quality control algorithm with improved cloud screening for Sun photometer aerosol optical depth (AOD) measurements, *Atmos. Meas. Tech.*, 12, 169–209, <https://doi.org/10.5194/amt-12-169-2019>, 2019.
- 1030 Ginoux, P., Garbuzov, D., and Hsu, N. C.: Identification of anthropogenic and natural dust sources using Moderate Resolution Imaging Spectroradiometer (MODIS) Deep Blue level 2 data, *J. Geophys. Res.-Atmos.*, 115, <https://doi.org/10.1029/2009JD012398>, 2010.
- Ginoux, P., Clarisse, L., Clerbaux, C., Coheur, P.-F., Dubovik, O., Hsu, N. C., and Van Damme, M.: Mixing of dust and NH<sub>3</sub> observed globally over anthropogenic dust sources, *Atmos. Chem. Phys.*, 12, 7351–7363, <https://doi.org/10.5194/acp-12-7351-2012>, 2012a.
- Ginoux, P., Prospero, J. M., Gill, T. E., Hsu, N. C., and Zhao, M.: Global-scale attribution of anthropogenic and natural dust sources and their 1035 emission rates based on MODIS Deep Blue aerosol products, *Rev. Geophys.*, 50, <https://doi.org/10.1029/2012RG000388>, 2012b.
- Gkikas, A., Hatzianastassiou, N., Mihalopoulos, N., Katsoulis, V., Kazadzis, S., Pey, J., Querol, X., and Torres, O.: The regime of intense desert dust episodes in the Mediterranean based on contemporary satellite observations and ground measurements, *Atmos. Chem. Phys.*, 13, 12 135–12 154, <https://doi.org/10.5194/acp-13-12135-2013>, 2013.
- Gkikas, A., Houssos, E. E., Lolis, C. J., Bartzokas, A., Mihalopoulos, N., and Hatzianastassiou, N.: Atmospheric circulation evolution related 1040 to desert-dust episodes over the Mediterranean, *Q. J. Roy. Meteor. Soc.*, 141, 1634–1645, <https://doi.org/10.1002/qj.2466>, 2015.
- Gkikas, A., Basart, S., Hatzianastassiou, N., Marinou, E., Amiridis, V., Kazadzis, S., Pey, J., Querol, X., Jorba, O., Gassó, S., and Baldasano, J. M.: Mediterranean intense desert dust outbreaks and their vertical structure based on remote sensing data, *Atmos. Chem. Phys.*, 16, 8609–8642, <https://doi.org/10.5194/acp-16-8609-2016>, 2016.
- Gkikas, A., Obiso, V., Pérez García-Pando, C., Jorba, O., Hatzianastassiou, N., Vendrell, L., Basart, S., Solomos, S., Gassó, S., and 1045 Baldasano, J. M.: Direct radiative effects during intense Mediterranean desert dust outbreaks, *Atmos. Chem. Phys.*, 18, 8757–8787, <https://doi.org/10.5194/acp-18-8757-2018>, 2018.
- Gkikas, A., Giannaros, T., Kotroni, V., and Lagouvardos, K.: Assessing the radiative impacts of an extreme desert dust outbreak and the potential improvements on short-term weather forecasts: The case of February 2015, *Atmos. Res.*, 226, 152–170, <https://doi.org/10.1016/j.atmosres.2019.04.020>, 2019.
- 1050 Gkikas, A., Proestakis, E., Amiridis, V., Kazadzis, S., Di Tomaso, E., Tsekeri, A., Marinou, E., Hatzianastassiou, N., and Pérez García-Pando, C.: ModIs Dust AeroSol (MIDAS): A global fine resolution dust optical depth dataset, Zenodo, <https://doi.org/10.5281/zenodo.4244106>, 2020.
- Gkikas, A., Proestakis, E., Amiridis, V., Kazadzis, S., Di Tomaso, E., Tsekeri, A., Marinou, E., Hatzianastassiou, N., and Pérez García-Pando, C.: ModIs Dust AeroSol (MIDAS): a global fine-resolution dust optical depth data set, *Atmos. Meas. Tech.*, 14, 309–334, 1055 <https://doi.org/10.5194/amt-14-309-2021>, 2021.
- Goossens, D. and Van Kerschaever, E.: Aeolian dust deposition on photovoltaic solar cells: the effects of wind velocity and airborne dust concentration on cell performance, *Sol. Energy*, 66, 277–289, [https://doi.org/10.1016/S0038-092X\(99\)00028-6](https://doi.org/10.1016/S0038-092X(99)00028-6), 1999.

- Goudie, A. S. and Middleton, N. J.: Desert Dust in the Global System, Springer Berlin, Heidelberg, 1<sup>st</sup> edn., <https://doi.org/10.1007/3-540-32355-4>, 2006.
- 1060 Griffin, D. W.: Atmospheric Movement of Microorganisms in Clouds of Desert Dust and Implications for Human Health, *Clin. Microbiol. Rev.*, 20, 459–477, <https://doi.org/10.1128/CMR.00039-06>, 2007.
- Guo, Y., Tian, B., Kahn, R. A., Kalashnikova, O., Wong, S., and Waliser, D. E.: Tropical Atlantic dust and smoke aerosol variations related to the Madden-Julian Oscillation in MODIS and MISR observations, *J. Geophys. Res.-Atmos.*, 118, 4947–4963, <https://doi.org/10.1002/jgrd.50409>, 2013.
- 1065 Gyan, K., Henry, W., Lacaille, S., Laloo, A., Lamsee-Ebanks, C., McKay, S., Antoine, R. M., and Monteil, M. A.: African dust clouds are associated with increased paediatric asthma accident and emergency admissions on the Caribbean island of Trinidad, *Int. J. Biometeorol.*, 49, 371–376, <https://doi.org/10.1007/s00484-005-0257-3>, 2005.
- Holben, B., Eck, T., Slutsker, I., Tanré, D., Buis, J., Setzer, A., Vermote, E., Reagan, J., Kaufman, Y., Nakajima, T., Lavenu, F., Jankowiak, I., and Smirnov, A.: AERONET—A Federated Instrument Network and Data Archive for Aerosol Characterization, *Remote Sens. Environ.*, 1070 66, 1–16, [https://doi.org/10.1016/S0034-4257\(98\)00031-5](https://doi.org/10.1016/S0034-4257(98)00031-5), 1998.
- Hsu, N. C., Tsay, S.-C., King, M. D., and Herman, J. R.: Aerosol properties over bright-reflecting source regions, *IEEE T. Geosci. Remote*, 42, 557–569, <https://doi.org/10.1109/TGRS.2004.824067>, 2004.
- Hunt, B. R., Kostelich, E. J., and Szunyogh, I.: Efficient data assimilation for spatiotemporal chaos: A local ensemble transform Kalman filter, *Physica D*, 230, 112–126, <https://doi.org/10.1016/j.physd.2006.11.008>, 2007.
- 1075 Inness, A., Baier, F., Benedetti, A., Bouarar, I., Chabrillat, S., Clark, H., Clerbaux, C., Coheur, P., Engelen, R. J., Errera, Q., Flemming, J., George, M., Granier, C., Hadji-Lazarou, J., Huijnen, V., Hurtmans, D., Jones, L., Kaiser, J. W., Kapsomenakis, J., Lefever, K., Leitão, J., Razinger, M., Richter, A., Schultz, M. G., Simmons, A. J., Suttie, M., Stein, O., Thépaut, J.-N., Thouret, V., Vrekoussis, M., Zerefos, C., and the MACC team: The MACC reanalysis: an 8 yr data set of atmospheric composition, *Atmos. Chem. Phys.*, 13, 4073–4109, <https://doi.org/10.5194/acp-13-4073-2013>, 2013.
- 1080 Inness, A., Ades, M., Agustí-Panareda, A., Barré, J., Benedictow, A., Blechschmidt, A.-M., Dominguez, J. J., Engelen, R., Eskes, H., Flemming, J., Huijnen, V., Jones, L., Kipling, Z., Massart, S., Parrington, M., Peuch, V.-H., Razinger, M., Remy, S., Schulz, M., and Suttie, M.: The CAMS reanalysis of atmospheric composition, *Atmos. Chem. Phys.*, 19, 3515–3556, <https://doi.org/10.5194/acp-19-3515-2019>, 2019.
- Jiang, H., Lu, L., and Sun, K.: Experimental investigation of the impact of airborne dust deposition on the performance of solar photovoltaic (PV) modules, *Atmos. Environ.*, 45, 4299–4304, <https://doi.org/10.1016/j.atmosenv.2011.04.084>, 2011.
- 1085 Jickells, T. D., An, Z. S., Andersen, K. K., Baker, A. R., Bergametti, G., Brooks, N., Cao, J. J., Boyd, P. W., Duce, R. A., Hunter, K. A., Kawahata, H., Kubilay, N., laRoche, J., Liss, P. S., Mahowald, N., Prospero, J. M., Ridgwell, A. J., Tegen, I., and Torres, R.: Global Iron Connections Between Desert Dust, Ocean Biogeochemistry, and Climate, *Science*, 308, 67–71, <https://doi.org/10.1126/science.1105959>, 2005.
- 1090 Kahn, R., West, R., McDonald, D., Rheingans, B., and Mishchenko, M. I.: Sensitivity of multiangle remote sensing observations to aerosol sphericity, *J. Geophys. Res.-Atmos.*, 102, 16 861–16 870, <https://doi.org/10.1029/96JD01934>, 1997.
- Kahn, R., Banerjee, P., McDonald, D., and Diner, D. J.: Sensitivity of multiangle imaging to aerosol optical depth and to pure-particle size distribution and composition over ocean, *J. Geophys. Res.-Atmos.*, 103, 32 195–32 213, <https://doi.org/10.1029/98JD01752>, 1998.
- Kahn, R., Banerjee, P., and McDonald, D.: Sensitivity of multiangle imaging to natural mixtures of aerosols over ocean, *J. Geophys. Res.-Atmos.*, 106, 18 219–18 238, <https://doi.org/10.1029/2000JD900497>, 2001.
- 1095

- Kahn, R. A. and Gaitley, B. J.: An analysis of global aerosol type as retrieved by MISR, *J. Geophys. Res.-Atmos.*, 120, 4248–4281, <https://doi.org/10.1002/2015JD023322>, 2015.
- Kahn, R. A., Gaitley, B. J., Garay, M. J., Diner, D. J., Eck, T. F., Smirnov, A., and Holben, B. N.: Multiangle Imaging Spectro-Radiometer global aerosol product assessment by comparison with the Aerosol Robotic Network, *J. Geophys. Res.-Atmos.*, 115, <https://doi.org/10.1029/2010JD014601>, 2010.
- 1100 Kalashnikova, O. V. and Kahn, R.: Ability of multiangle remote sensing observations to identify and distinguish mineral dust types: 2. Sensitivity over dark water, *J. Geophys. Res.-Atmos.*, 111, <https://doi.org/10.1029/2005JD006756>, 2006.
- Kalashnikova, O. V. and Kahn, R. A.: Mineral dust plume evolution over the Atlantic from MISR and MODIS aerosol retrievals, *J. Geophys. Res.-Atmos.*, 113, <https://doi.org/10.1029/2008JD010083>, 2008.
- 1105 Kalashnikova, O. V., Garay, M. J., Martonchik, J. V., and Diner, D. J.: MISR Dark Water aerosol retrievals: operational algorithm sensitivity to particle non-sphericity, *Atmos. Meas. Tech.*, 6, 2131–2154, <https://doi.org/10.5194/amt-6-2131-2013>, 2013.
- Kaly, F., Marticorena, B., Chatenet, B., Rajot, J., Janicot, S., Niang, A., Yahi, H., Thiria, S., Maman, A., Zakou, A., Coulibaly, B., Coulibaly, M., Koné, I., Traoré, S., Diallo, A., and Ndiaye, T.: Variability of mineral dust concentrations over West Africa monitored by the Sahelian Dust Transect, *Atmos. Res.*, 164–165, 226–241, <https://doi.org/10.1016/j.atmosres.2015.05.011>, 2015.
- 1110 Kanatani, K. T., Ito, I., Al-Delaimy, W. K., Adachi, Y., Mathews, W. C., and Ramsdell, J. W.: Desert dust exposure is associated with increased risk of asthma hospitalization in children, *Am. J. Resp. Crit. Care*, 182, 1475–1481, <https://doi.org/10.1164/rccm.201002-0296OC>, 2010.
- Karydis, V. A., Tsimpidi, A. P., Bacer, S., Pozzer, A., Nenes, A., and Lelieveld, J.: Global impact of mineral dust on cloud droplet number concentration, *Atmos. Chem. Phys.*, 17, 5601–5621, <https://doi.org/10.5194/acp-17-5601-2017>, 2017.
- Kaufman, Y. J., Koren, I., Remer, L. A., Tanré, D., Ginoux, P., and Fan, S.: Dust transport and deposition observed from the Terra-Moderate Resolution Imaging Spectroradiometer (MODIS) spacecraft over the Atlantic Ocean, *J. Geophys. Res.-Atmos.*, 110, <https://doi.org/10.1029/2003JD004436>, 2005.
- 1115 Klose, M., Jorba, O., Gonçalves Ageitos, M., Escribano, J., Dawson, M. L., Obiso, V., Di Tomaso, E., Basart, S., Montané Pinto, G., Macchia, F., Ginoux, P., Guerschman, J., Prigent, C., Huang, Y., Kok, J. F., Miller, R. L., and Pérez García-Pando, C.: Mineral dust cycle in the Multiscale Online Nonhydrostatic Atmosphere Chemistry model (MONARCH) Version 2.0, *Geosci. Model Dev.*, 14, 6403–6444, <https://doi.org/10.5194/gmd-14-6403-2021>, 2021.
- 1120 Kok, J. F., Ridley, D. A., Zhou, Q., Miller, R. L., Zhao, C., Heald, C. L., Ward, D. S., Albani, S., and Haustein, K.: Smaller desert dust cooling effect estimated from analysis of dust size and abundance, *Nat. Geosci.*, 10, 274–278, <https://doi.org/10.1038/ngeo2912>, 2017.
- Kosmopoulos, P. G., Kazadzis, S., El-Askary, H., Taylor, M., Gkikas, A., Proestakis, E., Kontoes, C., and El-Khayat, M. M.: Earth-observation-based estimation and forecasting of particulate matter impact on solar energy in Egypt, *Remote Sens.*, 10, <https://doi.org/10.3390/rs10121870>, 2018.
- 1125 Lambert, F., Kug, J.-S., Park, R. J., Mahowald, N., Winckler, G., Abe-Ouchi, A., O’ishi, R., Takemura, T., and Lee, J.-H.: The role of mineral-dust aerosols in polar temperature amplification, *Nat. Clim. Change*, 3, 487–491, <https://doi.org/10.1038/nclimate1785>, 2013.
- Lekas, T. I., Kushta, J., Solomos, S., and Kallos, G.: Some considerations related to flight in dusty conditions, *Journal of Aerospace Operations*, 3, 45–56, <https://doi.org/10.3233/AOP-140043>, 2014.
- 1130 Lekunberri, I., Lefort, T., Romero, E., Vázquez-Domínguez, E., Romera-Castillo, C., Marrasé, C., Peters, F., Weinbauer, M., and Gasol, J. M.: Effects of a dust deposition event on coastal marine microbial abundance and activity, bacterial community structure and ecosystem function, *J. Plankton Res.*, 32, 381–396, <https://doi.org/10.1093/plankt/fbp137>, 2010.

- Levin, Z., Ganor, E., and Gladstein, V.: The effects of desert particles coated with sulfate on rain formation in the Eastern Mediterranean, *J. Appl. Meteorol. Clim.*, 35, 1511–1523, [https://doi.org/10.1175/1520-0450\(1996\)035<1511:TEODPC>2.0.CO;2](https://doi.org/10.1175/1520-0450(1996)035<1511:TEODPC>2.0.CO;2), 1996.
- 1135 Liu, D., Wang, Z., Liu, Z., Winker, D., and Trepte, C.: A height resolved global view of dust aerosols from the first year CALIPSO lidar measurements, *J. Geophys. Res.-Atmos.*, 113, <https://doi.org/10.1029/2007JD009776>, 2008.
- Liu, D., Taylor, J. W., Crosier, J., Marsden, N., Bower, K. N., Lloyd, G., Ryder, C. L., Brooke, J. K., Cotton, R., Marengo, F., Blyth, A., Cui, Z., Estelles, V., Gallagher, M., Coe, H., and Choulaton, T. W.: Aircraft and ground measurements of dust aerosols over the west African coast in summer 2015 during ICE-D and AER-D, *Atmos. Chem. Phys.*, 18, 3817–3838, <https://doi.org/10.5194/acp-18-3817-2018>, 2018.
- 1140 Lynch, P., Reid, J. S., Westphal, D. L., Zhang, J., Hogan, T. F., Hyer, E. J., Curtis, C. A., Hegg, D. A., Shi, Y., Campbell, J. R., Rubin, J. I., Sessions, W. R., Turk, F. J., and Walker, A. L.: An 11-year global gridded aerosol optical thickness reanalysis (v1.0) for atmospheric and climate sciences, *Geosci. Model Dev.*, 9, 1489–1522, <https://doi.org/10.5194/gmd-9-1489-2016>, 2016.
- Mahowald, N., Albani, S., Kok, J. F., Engelstaeder, S., Scanza, R., Ward, D. S., and Flanner, M. G.: The size distribution of desert dust aerosols and its impact on the Earth system, *Aeolian Res.*, 15, 53–71, <https://doi.org/10.1016/j.aeolia.2013.09.002>, 2014.
- 1145 Mallone, S., Stafoggia, M., Faustini, A., Gobbi, G. P., Marconi, A., and Forastiere, F.: Saharan dust and associations between particulate matter and daily mortality in Rome, Italy, *Environ. Health Persp.*, 119, 1409–1414, <https://doi.org/10.1289/ehp.1003026>, 2011.
- Mani, M. and Pillai, R.: Impact of dust on solar photovoltaic (PV) performance: Research status, challenges and recommendations, *Renewable and Sustainable Energy Reviews*, 14, 3124–3131, <https://doi.org/10.1016/j.rser.2010.07.065>, 2010.
- Marinou, E., Amiridis, V., Biniotoglou, I., Tsikerdekis, A., Solomos, S., Proestakis, E., Konsta, D., Papagiannopoulos, N., Tsekeri, A., Vlastou, G., Zanis, P., Balis, D., Wandinger, U., and Ansmann, A.: Three-dimensional evolution of Saharan dust transport towards Europe based on a 9-year EARLINET-optimized CALIPSO dataset, *Atmos. Chem. Phys.*, 17, 5893–5919, <https://doi.org/10.5194/acp-17-5893-2017>, 2017.
- Middleton, N.: Desert dust hazards: A global review, *Aeolian Res.*, 24, 53–63, <https://doi.org/10.1016/j.aeolia.2016.12.001>, 2017.
- Middleton, N. J. and Goudie, A. S.: Saharan dust: sources and trajectories, *T. I. Brit. Geogr.*, 26, 165–181, <https://doi.org/10.1111/1475-1155.5661.00013>, 2001.
- 1155 Miller, R. L., Cakmur, R. V., Perlwitz, J., Geogdzhayev, I. V., Ginoux, P., Koch, D., Kohfeld, K. E., Prigent, C., Ruedy, R., Schmidt, G. A., and Tegen, I.: Mineral dust aerosols in the NASA Goddard Institute for Space Sciences ModelE atmospheric general circulation model, *J. Geophys. Res.-Atmos.*, 111, <https://doi.org/10.1029/2005JD005796>, 2006.
- Miri, A. and Middleton, N.: Long-term impacts of dust storms on transport systems in south-eastern Iran, *Nat. Hazards*, <https://doi.org/10.1007/s11069-022-05390-z>, 2022.
- 1160 Miyoshi, T. and Yamane, S.: Local ensemble transform Kalman filtering with an AGCM at a T159/L48 resolution, *Mon. Weather Rev.*, 135, 3841–3861, <https://doi.org/10.1175/2007MWR1873.1>, 2007.
- Mona, L., Amodeo, A., Pandolfi, M., and Pappalardo, G.: Saharan dust intrusions in the Mediterranean area: Three years of Raman lidar measurements, *J. Geophys. Res.-Atmos.*, 111, <https://doi.org/10.1029/2005JD006569>, 2006.
- 1165 Monteiro, A., Basart, S., Kazadzis, S., Votzis, A., Gkikas, A., Vandembussche, S., Tobias, A., Gama, C., García-Pando, C. P., Terradellas, E., Notas, G., Middleton, N., Kushta, J., Amiridis, V., Lagouvardos, K., Kosmopoulos, P., Kotroni, V., Kanakidou, M., Mihalopoulos, N., Kalivitis, N., Dagsson-Waldhauserová, P., El-Askary, H., Sievers, K., Giannaros, T., Mona, L., Hirtl, M., Skomorowski, P., Virtanen, T. H., Christoudias, T., Di Mauro, B., Trippetta, S., Kutuzov, S., Meinander, O., and Nickovic, S.: Multi-sectoral impact assessment of an extreme African dust episode in the Eastern Mediterranean in March 2018, *Sci. Total Environ.*, 843, 156861, <https://doi.org/10.1016/j.scitotenv.2022.156861>, 2022.
- 1170

- Myhre, G. and Stordal, F.: Global sensitivity experiments of the radiative forcing due to mineral aerosols, *J. Geophys. Res.-Atmos.*, 106, 18 193–18 204, <https://doi.org/10.1029/2000JD900536>, 2001.
- 1175 Myhre, G., Shindell, D., Bréon, F.-M., Collins, W., Fuglestedt, J., Huang, J., Koch, D., Lamarque, J.-F., Lee, D., Mendoza, B., Nakajima, T., Robock, A., Stephens, G., Takemura, T., and Zhang, H.: Anthropogenic and Natural Radiative Forcing, in: *Climate Change 2013: The Physical Science Basis. Contribution of Working Group I to the Fifth Assessment Report of the Intergovernmental Panel on Climate Change*, edited by Stocker, T. F., Qin, D., Plattner, G.-K., Tignor, M., Allen, S., Boschung, J., Nauels, A., Xia, Y., Bex, V., and Midgley, P. M., chap. 8, pp. 659–740, Cambridge University Press, Cambridge, United Kingdom and New York, NY, USA, 2013.
- 1180 Nabat, P., Somot, S., Mallet, M., Michou, M., Sevault, F., Driouech, F., Meloni, D., di Sarra, A., Di Biagio, C., Formenti, P., Sicard, M., Léon, J.-F., and Bouin, M.-N.: Dust aerosol radiative effects during summer 2012 simulated with a coupled regional aerosol–atmosphere–ocean model over the Mediterranean, *Atmos. Chem. Phys.*, 15, 3303–3326, <https://doi.org/10.5194/acp-15-3303-2015>, 2015.
- Okin, G. S., Mahowald, N., Chadwick, O. A., and Artaxo, P.: Impact of desert dust on the biogeochemistry of phosphorus in terrestrial ecosystems, *Global Biogeochem. Cy.*, 18, <https://doi.org/10.1029/2003GB002145>, 2004.
- O’Neill, N. T., Eck, T. F., Smirnov, A., Holben, B. N., and Thulasiraman, S.: Spectral discrimination of coarse and fine mode optical depth, *J. Geophys. Res.-Atmos.*, 108, <https://doi.org/10.1029/2002JD002975>, 2003.
- 1185 Painter, T. H., Barrett, A. P., Landry, C. C., Neff, J. C., Cassidy, M. P., Lawrence, C. R., McBride, K. E., and Farmer, G. L.: Impact of disturbed desert soils on duration of mountain snow cover, *Geophys. Res. Lett.*, 34, <https://doi.org/10.1029/2007GL030284>, 2007.
- Papagiannopoulos, N., Mona, L., Amodeo, A., D’Amico, G., Gumà Claramunt, P., Pappalardo, G., Alados-Arboledas, L., Guerrero-Rascado, J. L., Amiridis, V., Kokkalis, P., Apituley, A., Baars, H., Schwarz, A., Wandinger, U., Biniotoglou, I., Nicolae, D., Bortoli, D., Comerón, A., Rodríguez-Gómez, A., Sicard, M., Papayannis, A., and Wiegner, M.: An automatic observation-based aerosol typing method for EARLINET, *Atmos. Chem. Phys.*, 18, 15 879–15 901, <https://doi.org/10.5194/acp-18-15879-2018>, 2018.
- 1190 Papayannis, A., Amiridis, V., Mona, L., Tsaknakis, G., Balis, D., Bösenberg, J., Chaikovski, A., De Tomasi, F., Grigorov, I., Mattis, I., Mitev, V., Müller, D., Nickovic, S., Pérez, C., Pietruczuk, A., Pisani, G., Ravetta, F., Rizi, V., Sicard, M., Trickl, T., Wiegner, M., Gerding, M., Mamouri, R. E., D’Amico, G., and Pappalardo, G.: Systematic lidar observations of Saharan dust over Europe in the frame of EARLINET (2000–2002), *J. Geophys. Res.-Atmos.*, 113, <https://doi.org/10.1029/2007JD009028>, 2008.
- 1195 Papayannis, A., Nicolae, D., Kokkalis, P., Biniotoglou, I., Talianu, C., Belegante, L., Tsaknakis, G., Cazacu, M., Vetres, I., and Ilic, L.: Optical, size and mass properties of mixed type aerosols in Greece and Romania as observed by synergy of lidar and sunphotometers in combination with model simulations: A case study, *Sci. Total Environ.*, 500-501, 277–294, <https://doi.org/10.1016/j.scitotenv.2014.08.101>, 2014.
- 1200 Pérez, C., Hausteine, K., Janjic, Z., Jorba, O., Huneeus, N., Baldasano, J. M., Black, T., Basart, S., Nickovic, S., Miller, R. L., Perlwitz, J. P., Schulz, M., and Thomson, M.: Atmospheric dust modeling from meso to global scales with the online NMMB/BSC-Dust model - Part 1: Model description, annual simulations and evaluation, *Atmos. Chem. Phys.*, 11, 13 001–13 027, <https://doi.org/10.5194/acp-11-13001-2011>, 2011.
- Pérez García-Pando, C., Stanton, M. C., Diggle, P. J., Trzaska, S., Miller, R. L., Perlwitz, J. P., Baldasano, J. M., Cuevas, E., Ceccato, P., Yaka, P., and Thomson, M. C.: Soil dust aerosols and wind as predictors of seasonal meningitis incidence in Niger, *Environ. Health Persp.*, 122, 679–686, <https://doi.org/10.1289/ehp.1306640>, 2014.
- 1205 Peyridieu, S., Chédin, A., Capelle, V., Tsamalis, C., Pierangelo, C., Armante, R., Crevoisier, C., Crépeau, L., Siméon, M., Ducos, F., and Scott, N. A.: Characterisation of dust aerosols in the infrared from IASI and comparison with PARASOL, MODIS, MISR, CALIOP, and AERONET observations, *Atmos. Chem. Phys.*, 13, 6065–6082, <https://doi.org/10.5194/acp-13-6065-2013>, 2013.



- Pierangelo, C., Mishchenko, M., Balkanski, Y., and Chédin, A.: Retrieving the effective radius of Saharan dust coarse mode from AIRS, 1210 *Geophys. Res. Lett.*, 32, <https://doi.org/10.1029/2005GL023425>, 2005.
- Pierce, J. R., Kahn, R. A., Davis, M. R., and Comstock, J. M.: Detecting thin cirrus in Multiangle Imaging Spectroradiometer aerosol retrievals, *J. Geophys. Res.-Atmos.*, 115, <https://doi.org/10.1029/2009JD013019>, 2010.
- Proestakis, E., Amiridis, V., Marinou, E., Georgoulas, A. K., Solomos, S., Kazadzis, S., Chimot, J., Che, H., Alexandri, G., Biniotoglou, I., Daskalopoulou, V., Kourtidis, K. A., de Leeuw, G., and van der A, R. J.: Nine-year spatial and temporal evolution of desert dust aerosols 1215 over South and East Asia as revealed by CALIOP, *Atmos. Chem. Phys.*, 18, 1337–1362, <https://doi.org/10.5194/acp-18-1337-2018>, 2018.
- Prospero, J. M.: Long-range transport of mineral dust in the global atmosphere: Impact of African dust on the environment of the southeastern United States, *P. Natl. Acad. Sci. USA*, 96, 3396–3403, <https://doi.org/10.1073/pnas.96.7.3396>, 1999.
- Prospero, J. M., Ginoux, P., Torres, O., Nicholson, S. E., and Gill, T. E.: Environmental characterization of global sources of atmospheric soil dust identified with the nimbus 7 Total Ozone Mapping Spectrometer (TOMS) absorbing aerosol product, *Rev. Geophys.*, 40, 2–1–2–31, 1220 <https://doi.org/10.1029/2000RG000095>, 2002.
- Pu, B. and Ginoux, P.: The impact of the Pacific Decadal Oscillation on springtime dust activity in Syria, *Atmos. Chem. Phys.*, 16, 13431–13448, <https://doi.org/10.5194/acp-16-13431-2016>, 2016.
- Querol, X., Tobías, A., Pérez, N., Karanasiou, A., Amato, F., Stafoggia, M., Pérez García-Pando, C., Ginoux, P., Forastiere, F., Gumy, S., Mudu, P., and Alastuey, A.: Monitoring the impact of desert dust outbreaks for air quality for health studies, *Environ. Int.*, 130, 104867, 1225 <https://doi.org/10.1016/j.envint.2019.05.061>, 2019.
- Ramaswamy, V., Muraleedharan, P. M., and Babu, C. P.: Mid-troposphere transport of Middle-East dust over the Arabian Sea and its effect on rainwater composition and sensitive ecosystems over India, *Sci. Rep.-UK*, 7, 13676, <https://doi.org/10.1038/s41598-017-13652-1>, 2017.
- Roberts, A. and Knippertz, P.: Haboobs: convectively generated dust storms in West Africa, *Weather*, 67, 311–316, <https://doi.org/10.1002/wea.1968>, 2012.
- 1230 Sayer, A. M., Munchak, L. A., Hsu, N. C., Levy, R. C., Bettenhausen, C., and Jeong, M.-J.: MODIS Collection 6 aerosol products: Comparison between Aqua's e-Deep Blue, Dark Target, and "merged" data sets, and usage recommendations, *J. Geophys. Res.-Atmos.*, 119, 13,965–13,989, <https://doi.org/10.1002/2014JD022453>, 2014.
- Schutgens, N. A. J., Miyoshi, T., Takemura, T., and Nakajima, T.: Applying an ensemble Kalman filter to the assimilation of AERONET observations in a global aerosol transport model, *Atmos. Chem. Phys.*, 10, 2561–2576, <https://doi.org/10.5194/acp-10-2561-2010>, 2010.
- 1235 Sinyuk, A., Dubovik, O., Holben, B., Eck, T. F., Breon, F.-M., Martonchik, J., Kahn, R., Diner, D. J., Vermote, E. F., Roger, J.-C., Lapyonok, T., and Slutsker, I.: Simultaneous retrieval of aerosol and surface properties from a combination of AERONET and satellite data, *Remote Sens. Environ.*, 107, 90–108, <https://doi.org/10.1016/j.rse.2006.07.022>, 2007.
- Sivakumar, M. V.: Impacts of Sand Storms/Dust Storms on Agriculture, in: *Natural Disasters and Extreme Events in Agriculture: Impacts and Mitigation*, edited by Sivakumar, M. V., Motha, R. P., and Das, H. P., pp. 159–177, Springer Berlin Heidelberg, Berlin, Heidelberg, 1240 [https://doi.org/10.1007/3-540-28307-2\\_10](https://doi.org/10.1007/3-540-28307-2_10), 2005.
- Slingo, A., Ackerman, T. P., Allan, R. P., Kassianov, E. I., McFarlane, S. A., Robinson, G. J., Barnard, J. C., Miller, M. A., Harries, J. E., Russell, J. E., and Dewitte, S.: Observations of the impact of a major Saharan dust storm on the atmospheric radiation balance, *Geophys. Res. Lett.*, 33, <https://doi.org/10.1029/2006GL027869>, 2006.
- Sogacheva, L., Popp, T., Sayer, A. M., Dubovik, O., Garay, M. J., Heckel, A., Hsu, N. C., Jethva, H., Kahn, R. A., Kolmonen, P., Kosmale, 1245 M., de Leeuw, G., Levy, R. C., Litvinov, P., Lyapustin, A., North, P., Torres, O., and Arola, A.: Merging regional and global aerosol optical

- depth records from major available satellite products, *Atmos. Chem. Phys.*, 20, 2031–2056, <https://doi.org/10.5194/acp-20-2031-2020>, 2020.
- Solomos, S., Kalivitis, N., Mihalopoulos, N., Amiridis, V., Kouvarakis, G., Gkikas, A., Biniotoglou, I., Tsekeri, A., Kazadzis, S., Kottas, M., Pradhan, Y., Proestakis, E., Nastos, P. T., and Marengo, F.: From tropospheric folding to Khamsin and Foehn winds: How atmospheric dynamics advanced a record-breaking dust episode in Crete, *Atmosphere*, 9, <https://doi.org/10.3390/atmos9070240>, 2018.
- 1250 Stefanski, R. and Sivakumar, M. V. K.: Impacts of sand and dust storms on agriculture and potential agricultural applications of a SDSWS, *IOP C. Ser. Earth and Env.*, 7, 012 016, <https://doi.org/10.1088/1755-1307/7/1/012016>, 2009.
- Tegen, I. and Lacis, A. A.: Modeling of particle size distribution and its influence on the radiative properties of mineral dust aerosol, *J. Geophys. Res.-Atmos.*, 101, 19 237–19 244, <https://doi.org/10.1029/95JD03610>, 1996.
- 1255 Tegen, I., Lacis, A. A., and Fung, I.: The influence on climate forcing of mineral aerosols from disturbed soils, *Nature*, 380, 419–422, <https://doi.org/10.1038/380419a0>, 1996.
- Tsikierdekis, A., Schutgens, N. A. J., and Hasekamp, O. P.: Assimilating aerosol optical properties related to size and absorption from POLDER/PARASOL with an ensemble data assimilation system, *Atmos. Chem. Phys.*, 21, 2637–2674, <https://doi.org/10.5194/acp-21-2637-2021>, 2021.
- 1260 UNCCD: Sand and Dust Storms Compendium: Information and Guidance on Assessing and Addressing the Risks, United Nations Convention to Combat Desertification, Bonn, Germany, <https://www.unccd.int/resources/publications/sand-and-dust-storms-compendium-information-and-guidance-assessing-and>, last access: 30 March 2023, 2022.
- Wei, J., Li, Z., Peng, Y., and Sun, L.: MODIS Collection 6.1 aerosol optical depth products over land and ocean: validation and comparison, *Atmos. Environ.*, 201, 428–440, <https://doi.org/10.1016/j.atmosenv.2018.12.004>, 2019.
- 1265 Weinzierl, B., Sauer, D., Minikin, A., Reitebuch, O., Dahlkötter, F., Mayer, B., Emde, C., Tegen, I., Gasteiger, J., Petzold, A., Veira, A., Kueppers, U., and Schumann, U.: On the visibility of airborne volcanic ash and mineral dust from the pilot’s perspective in flight, *Phys. Chem. Earth Pt. A/B/C*, 45-46, 87–102, <https://doi.org/10.1016/j.pce.2012.04.003>, 2012.
- WHO: WHO global air quality guidelines: particulate matter (PM<sub>2.5</sub> and PM<sub>10</sub>), ozone, nitrogen dioxide, sulfur dioxide and carbon monoxide, World Health Organization, <https://apps.who.int/iris/handle/10665/345329>, last access: 30 March 2023, 2021.
- 1270 Winker, D. M., Vaughan, M. A., Omar, A., Hu, Y., Powell, K. A., Liu, Z., Hunt, W. H., and Young, S. A.: Overview of the CALIPSO mission and CALIOP data processing algorithms, *J. Atmos. Ocean. Tech.*, 26, 2310–2323, <https://doi.org/10.1175/2009JTECHA1281.1>, 2009.
- WMO: Plan for the implementation of the GAW Aerosol Lidar Observation Network (GALION), Tech. Rep. WMO/TD-No. 1443; GAW Report-No. 178, WMO, Hamburg, Germany, [https://library.wmo.int/doc\\_num.php?explnum\\_id=9387](https://library.wmo.int/doc_num.php?explnum_id=9387), last access: 30 March 2023, 2007.
- Yu, H., Chin, M., Yuan, T., Bian, H., Remer, L. A., Prospero, J. M., Omar, A., Winker, D., Yang, Y., Zhang, Y., Zhang, Z., and Zhao, C.: 1275 The fertilizing role of African dust in the Amazon rainforest: A first multiyear assessment based on data from Cloud-Aerosol Lidar and Infrared Pathfinder Satellite Observations, *Geophys. Res. Lett.*, 42, 1984–1991, <https://doi.org/10.1002/2015GL063040>, 2015.
- Yu, H., Tan, Q., Zhou, L., Zhou, Y., Bian, H., Chin, M., Ryder, C. L., Levy, R. C., Pradhan, Y., Shi, Y., Song, Q., Zhang, Z., Colarco, P. R., Kim, D., Remer, L. A., Yuan, T., Mayol-Bracero, O., and Holben, B. N.: Observation and modeling of the historic “Godzilla” African dust intrusion into the Caribbean Basin and the southern US in June 2020, *Atmos. Chem. Phys.*, 21, 12 359–12 383, <https://doi.org/10.5194/acp-21-12359-2021>, 2021.
- 1280 Yumimoto, K., Tanaka, T. Y., Oshima, N., and Maki, T.: JRAero: the Japanese Reanalysis for Aerosol v1.0, *Geosci. Model Dev.*, 10, 3225–3253, <https://doi.org/10.5194/gmd-10-3225-2017>, 2017.

Zender, C. S., Miller, R. L. L., and Tegen, I.: Quantifying mineral dust mass budgets: Terminology, constraints, and current estimates, *Eos Trans. AGU*, 85, 509–512, <https://doi.org/10.1029/2004EO480002>, 2004.

Validation of MIDAS and MISR DOD with AERONET

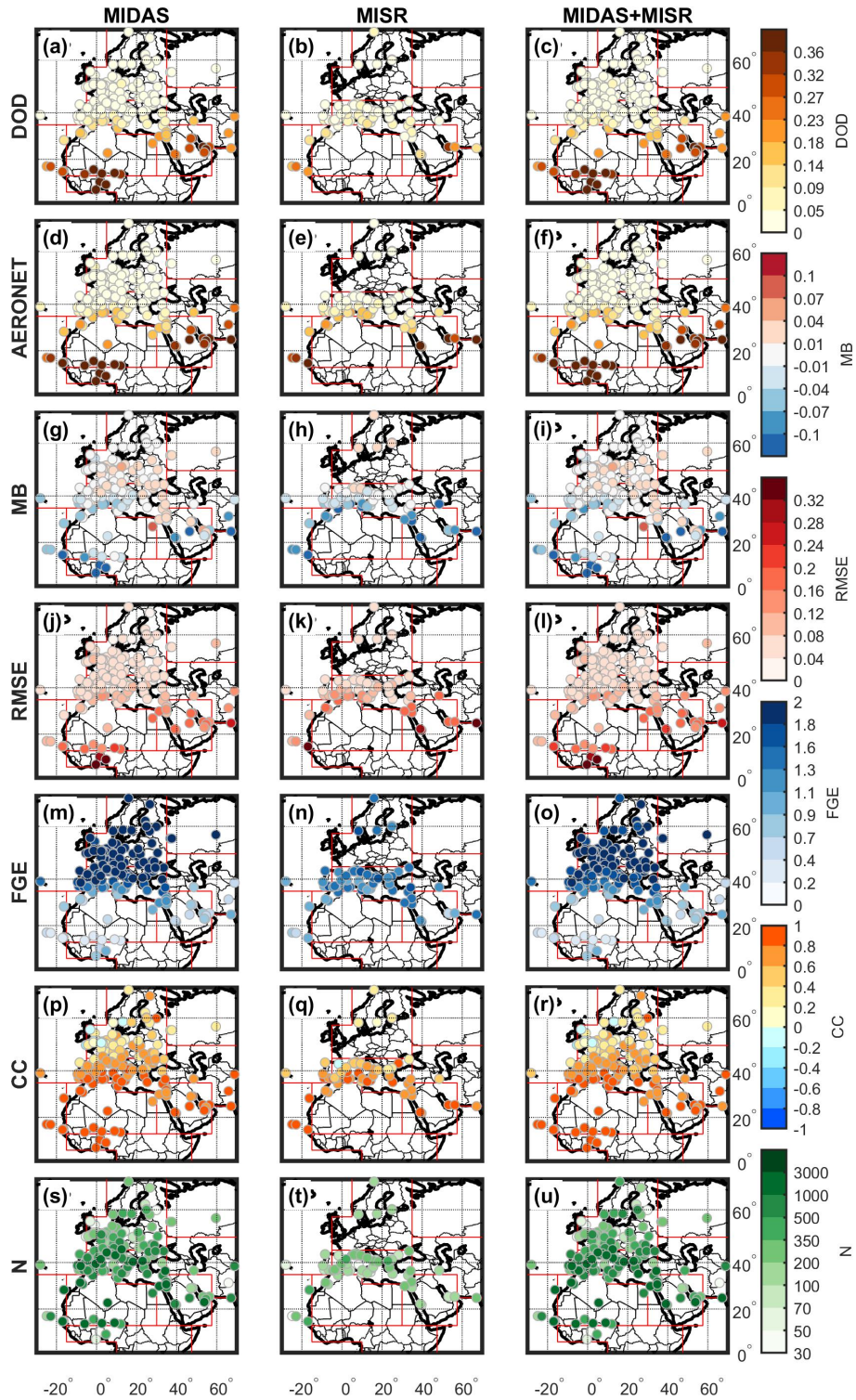


**Figure 2.** DOD comparison of MIDAS (1<sup>st</sup> column), MISR (2<sup>nd</sup> column) and MIDAS+MISR (3<sup>rd</sup> column) against AERONET for the period 2007–2016. The metrics MB, RMSE, FGE and CC (Table A1) were computed at station level. The obtained scores are presented here only for sites with  $N \geq 30$  collocated pairs. The red frames in the background delimit the sub-regions defined in Fig. 1.



Validation of MIDAS and AEROIASI coarse DOD with AERONET

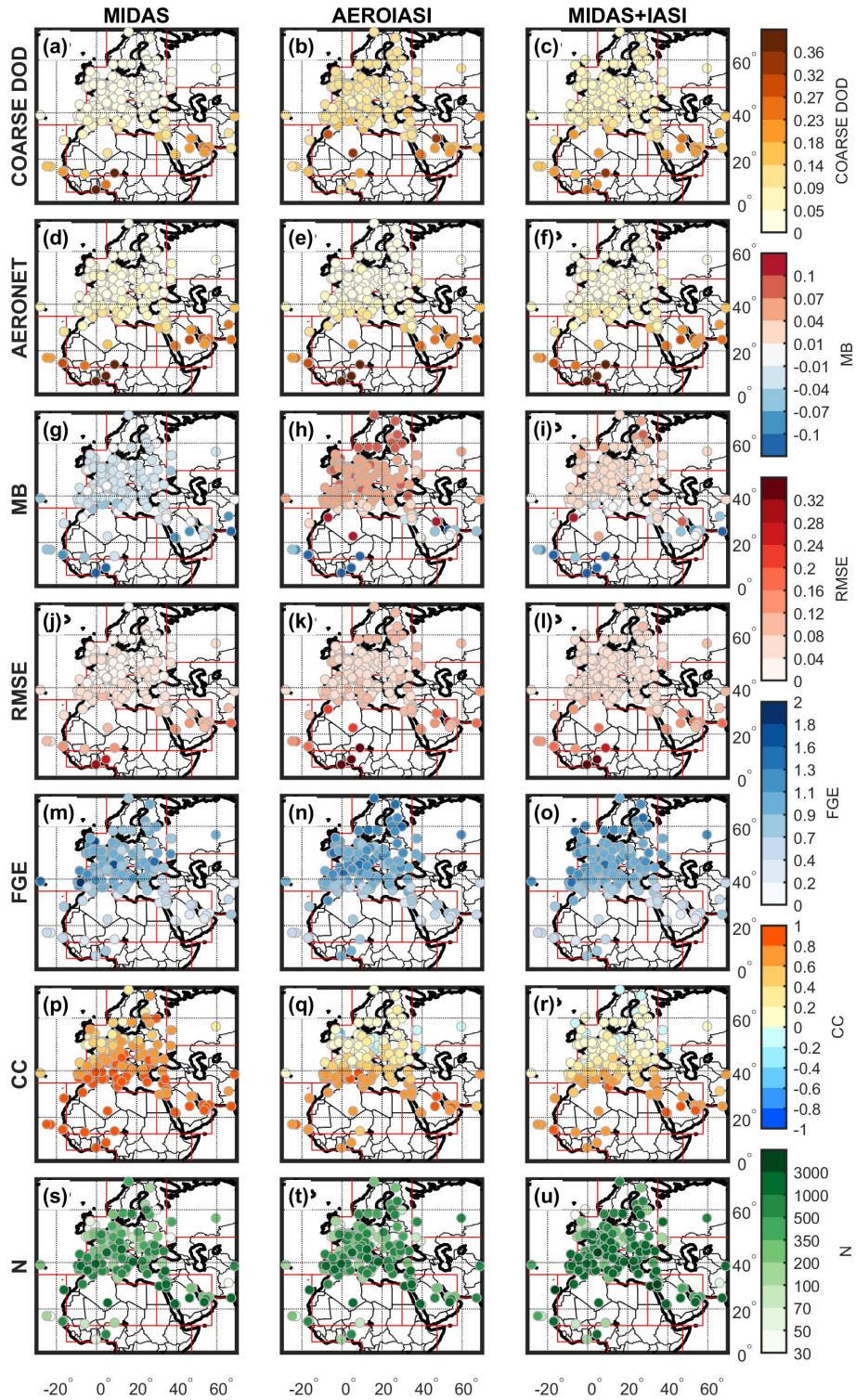


**Figure 3.** Coarse DOD comparison of MIDAS (1<sup>st</sup> column), AEROIASI (2<sup>nd</sup> column) and MIDAS+IASI (3<sup>rd</sup> column) against AERONET for the period 2007–2016. The metrics MB, RMSE, FGE and CC (Table A1) were computed at station level. The obtained scores are presented here only for sites with  $N \geq 30$  collocated pairs. The red frames in the background delimit the sub-regions defined in Fig. 1.

Comparison of MONARCH DOD with MIDAS, MISR and AERONET

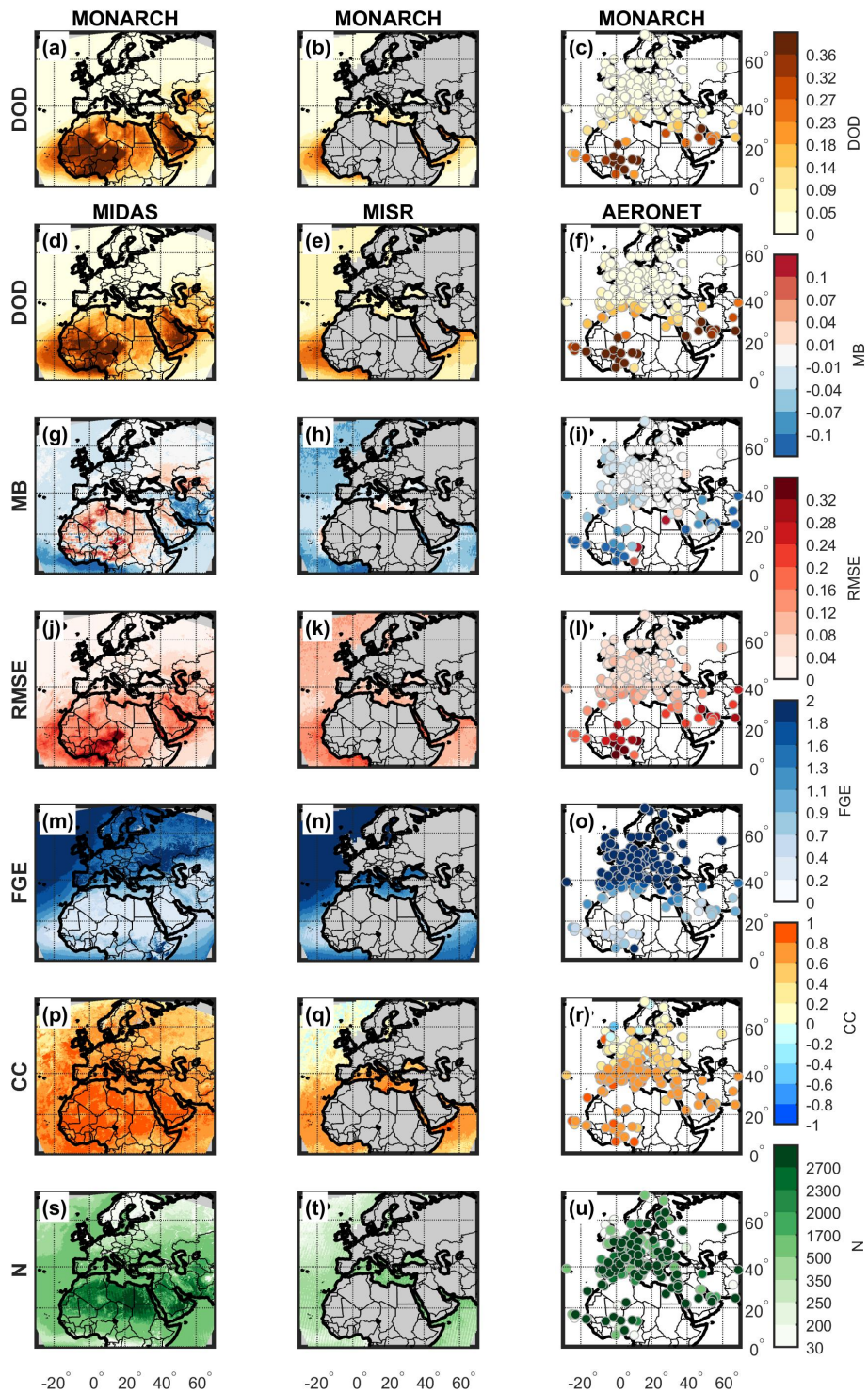


**Figure 4.** Spatial distribution of the total DOD simulated by the MONARCH reanalysis (a, e and e-a-c) and collocated with observations by MIDAS (b, d), MISR (e) and AERONET (f), along with the respective statistic parameters: MB (g-i), RMSE (j-l), FGE (m-o) and CC (p-r). Number N gives the total number of pairs collocated during the study period 2007–2016, at grid (s and t) and station level (u).



Comparison of MONARCH coarse DOD with MIDAS, AEROIASI and AERONET

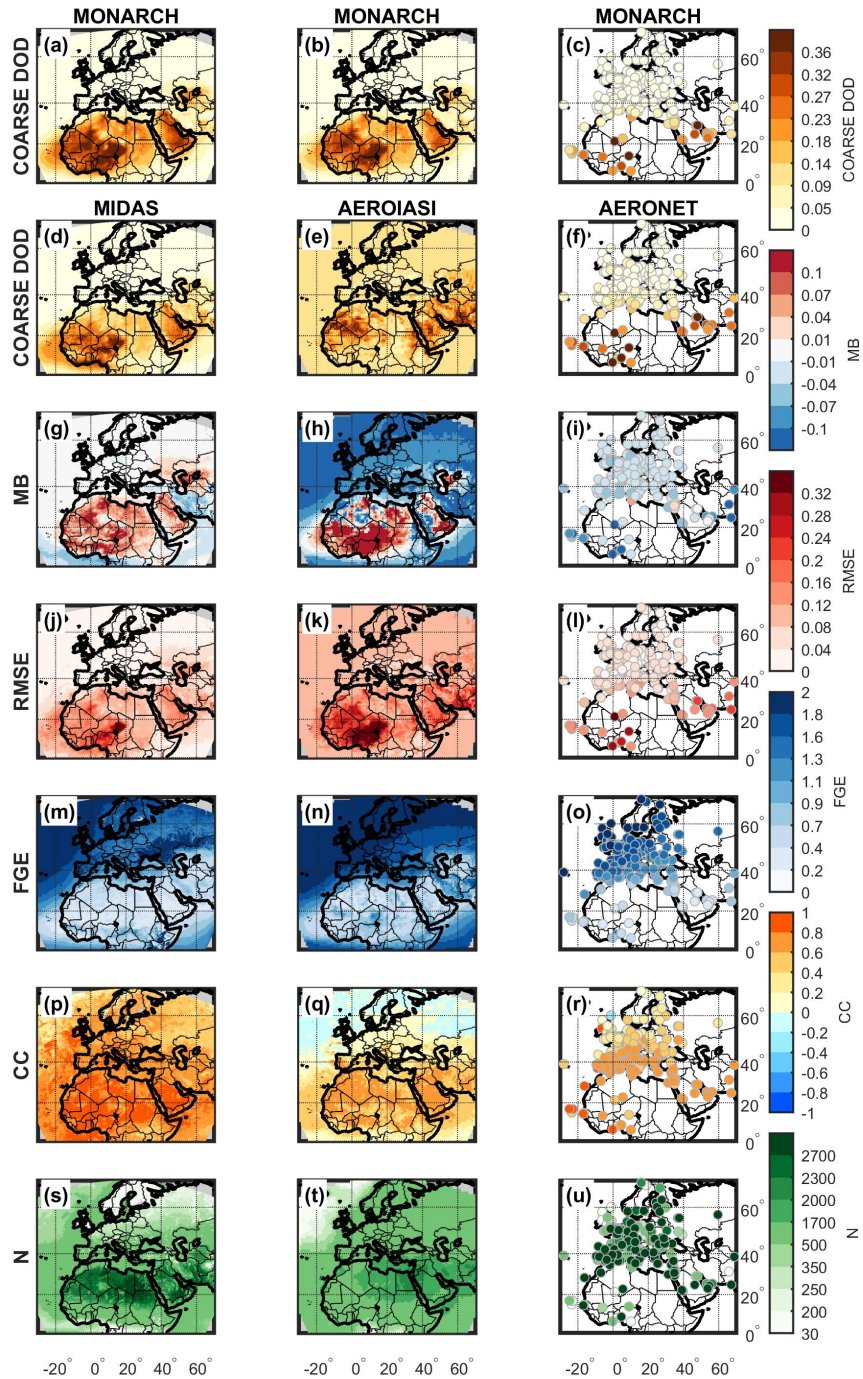


**Figure 5.** Spatial distribution of the coarse DOD simulated by the MONARCH reanalysis (a, c and e) and collocated with observations by MIDAS (b, d), AEROIASI (g, h, i) and AERONET (f), along with the respective statistic parameters: MB (g–i), RMSE (j–l), FGE (m–o) and CC (p–r). Number N gives the total number of pairs collocated during the study period 2007–2016, at grid (s and t) and station level (u).

Comparison between MONARCH and MIDAS+MISR DOD at regional level

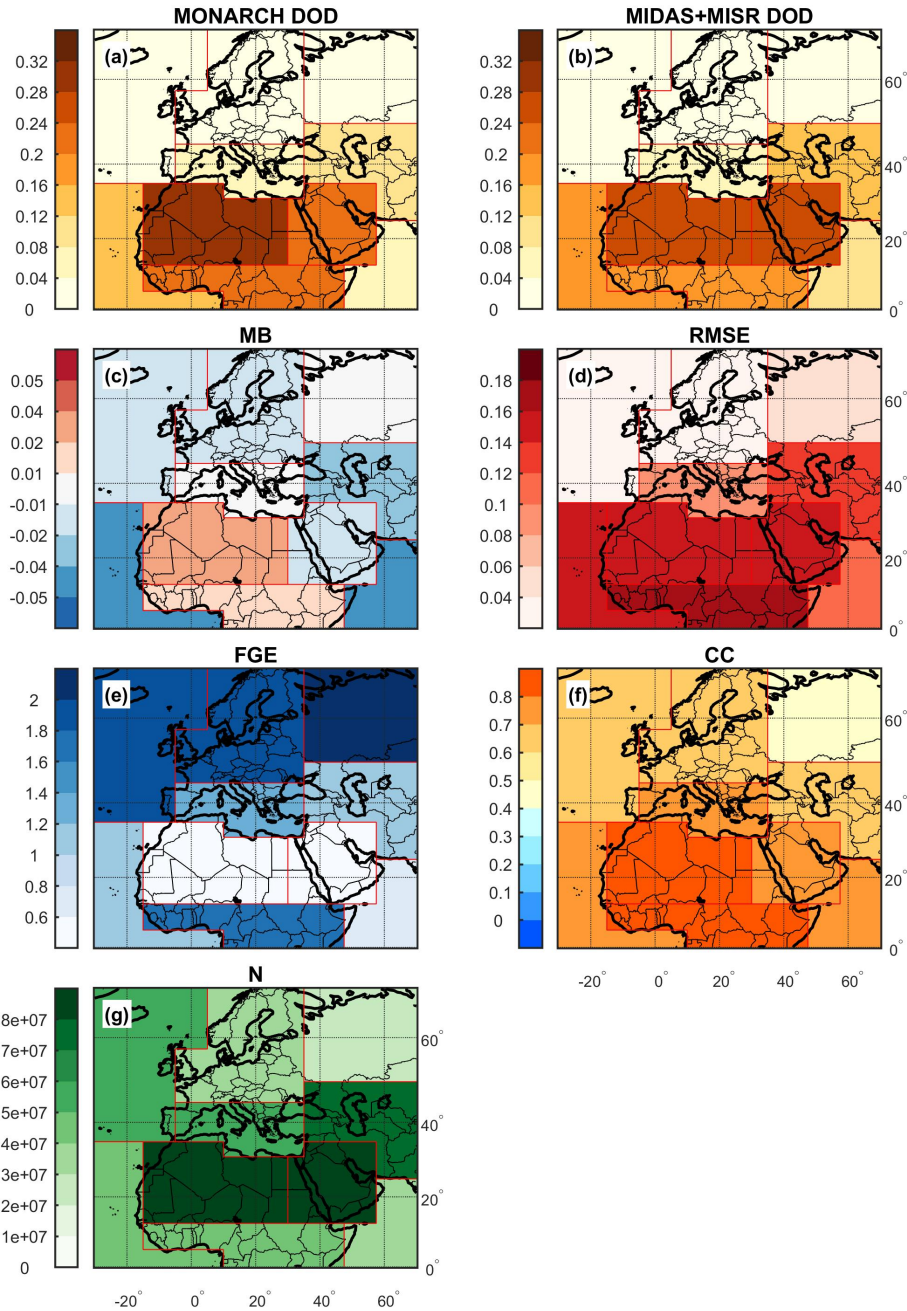


**Figure 6.** Regional weighted annual mean of the MONARCH reanalysis DOD (a), the MIDAS+MISR DOD (b), and their MB (c), RMSE (d), FGE (e) and CC (f) along with the total regional N (g). The results refer to the study period 2007–2016.

Comparison between MONARCH and MIDAS+IASI coarse DOD at regional level

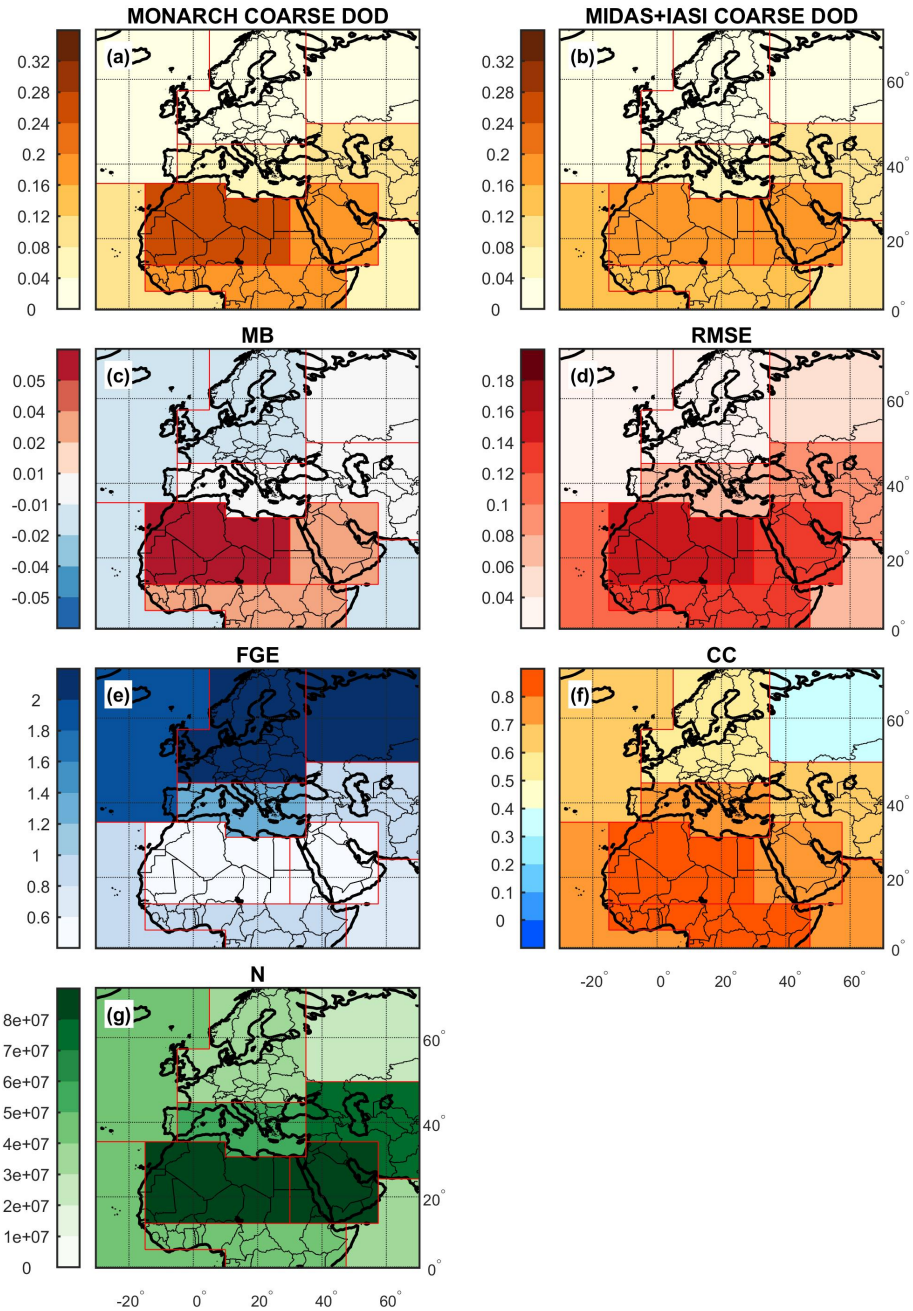


**Figure 7.** Regional weighted annual mean of the MONARCH reanalysis coarse DOD (a), the MIDAS+IASI coarse DOD (b), and their MB (c), RMSE (d), FGE (e) and CC (f) along with the total regional N (g). The results refer to the study period 2007–2016.